



Contents lists available at ScienceDirect

## Journal of Theoretical Biology

journal homepage: [www.elsevier.com/locate/yjtbi](http://www.elsevier.com/locate/yjtbi)

## Calsequestrin mediates changes in spontaneous calcium release profiles

Nessy Tania <sup>\*,1</sup>, James P. Keener

Department of Mathematics, University of Utah, 155 S. 1400 E. Room 233, Salt Lake City, UT 84112, USA

## ARTICLE INFO

## Article history:

Received 8 January 2010

Received in revised form

17 May 2010

Accepted 21 May 2010

Available online 2 June 2010

## Keywords:

Calcium spark

Ryanodine receptors

Luminal sensing

## ABSTRACT

Calsequestrin (CSQ) is the primary calcium buffer within the sarcoplasmic reticulum (SR) of cardiac cells. It has also been identified as a regulator of Ryanodine receptor (RyR) calcium release channels by serving as a SR luminal sensor. When calsequestrin is free and unbound to calcium, it can bind to RyR and desensitize the channel from cytoplasmic calcium activation. In this paper, we study the role of CSQ as a buffer and RyR luminal sensor using a mechanistic model of RyR–CSQ interaction. By using various asymptotic approximations and mean first exit time calculation, we derive a minimal model of a calcium release unit which includes CSQ dependence. Using this model, we then analyze the effect of changing CSQ expression on the calcium release profile and the rate of spontaneous calcium release. We show that because of its buffering capability, increasing CSQ increases the spark duration and size. However, because of luminal sensing effects, increasing CSQ depresses the basal spark rate and increases the critical SR level for calcium release termination. Finally, we show that with increased bulk cytoplasmic calcium concentration, the CRU model exhibits deterministic oscillations.

© 2010 Elsevier Ltd. All rights reserved.

## 1. Introduction

Under normal circumstances, the contractile activity of a cardiac myocyte is completely controlled by a propagating electrical signal known as an action potential. Calcium mediates this excitation–contraction coupling process and release occurs through a mechanism known as calcium-induced calcium release (CICR). The level of myoplasmic calcium concentration must be tightly regulated as disturbances in its regulation may decrease the cardiac pumping efficiency. Moreover, a spontaneous calcium release can trigger an action potential.

Mathematical models have been widely used to study calcium regulation in various cell types. However, the multiscale nature of the system presents a significant challenge in building tractable and useful models of calcium regulation at the whole-cell or tissue level. In the presence of positive feedback and high gain, local control is the sole mechanism in keeping the calcium-induced calcium release process in check. Thus, whole-cell calcium release is inherently spatially localized and stochastic in nature. Recent modeling efforts have focused on calcium regulation at a small patch-size or a release unit level (Greenstein et al., 2006; Hinch, 2004; Hinch et al., 2004; Tanskannen et al., 2007; Thul and Falcke, 2006). In this paper, we build upon these previous efforts and derive a minimal model for a calcium release

unit (CRU). This reduced description is then used to study the rates and properties of spontaneous calcium releases ( $\text{Ca}^{2+}$  spark). Specifically, we investigate how the level of expressions of calsequestrin, a buffer and a regulator of the calcium releases channels, changes nature of calcium release.

## 1.1. Calcium release in cardiac cells

During an action potential, voltage-gated L-type calcium channels (LCC) are activated as the cell membrane becomes depolarized. The resulting influx of calcium then serves as a trigger for more calcium to be released through ryanodine receptors (RyR) which are found on the surface of the sarcoplasmic reticulum (SR), an organelle that serves as a large calcium pool. The calcium-induced calcium release (CICR) mechanism exhibits a high degree of positive feedback and high gain in that the amount of calcium released from the SR is much larger than the input influx through the LCC. Because of positive feedback and high gain, the control of the CICR process appears to be impossible. However, in a normal cell, the process is clearly regulated as calcium release is graded in that the amount of calcium released is proportional to the influx amount. An important regulatory mechanism that allows for graded response is known as local control where calcium release occurs as a spatially localized event that does not spread to neighboring sites under normal physiological conditions (Stern, 1992).

A cell contains a large number of calcium release units (CRU), each of which consists of a separate diadic space and a junctional

\* Corresponding author. Tel.: +1 604 822 6754; fax: +1 604 822 6074.

E-mail address: [tania@math.utah.edu](mailto:tania@math.utah.edu) (N. Tania).

<sup>1</sup> Present address: Department of Mathematics, University of British Columbia, Room 121, 1984 Mathematics Road, Vancouver, Canada BC V6T 1Z2.

SR (JSR) compartment. Within a diadic space, an individual LCCs can interact with apposing RyRs. Because of positive feedback, an individual CRU responds in an all-or-none manner. The units can also possibly affect one another through calcium diffusion within the common bulk myoplasmic space and network SR (NSR). Recently, computational models that include these features of calcium handling have been used to simulate graded response under high gain in a mechanistic manner (Greenstein and Winslow, 2002; Rice et al., 2002; Sobie et al., 2002; Stern, 1992). To do so, large-scale Monte Carlo simulations of single channel dynamics within each CRU are performed with the result that these studies are computationally demanding. To keep computational run-times reasonable, the number of CRUs simulated is usually much smaller than the actual number found within a cell. Additionally, the large computational cost makes extensive studies of a variety of physiological conditions unfeasible. In particular, it is difficult to assess the occurrence of rare events from these stochastic simulations.

Hinch and others have presented a framework for building intracellular  $\text{Ca}^{2+}$  models that are computationally minimal but still capture the underlying local control nature of the process (Greenstein et al., 2006; Hinch, 2004; Hinch and Chapman, 2005; Hinch et al., 2004; Williams et al., 2007). Hinch showed that the calcium release in a CRU constitutes an excitable system (Hinch, 2004; Hinch and Chapman, 2005). Then, using various asymptotic timescale reductions and utilizing the law of large numbers, a deterministic model of  $\text{Ca}^{2+}$  release which consists of ordinary differential equations is built. The authors show that their mechanistic model exhibits graded response with high gain (Greenstein et al., 2006; Hinch et al., 2004). In these models, however, the diadic  $\text{Ca}^{2+}$  concentration is assumed to be dependent on the bulk NSR  $\text{Ca}^{2+}$  rather than the local JSR level. A generalization by Williams et al. (2007) allows for the previous assumption to be removed. The resulting model is composed of a system of Fokker–Planck equations describing the probability density function for the JSR  $\text{Ca}^{2+}$  concentration in the CRU. All of these models are useful in that they are computationally cheaper to simulate than large-scale Monte Carlo simulations and most importantly, they can be used to study the probability of rare spontaneous calcium release events.

### 1.2. The role of calsequestrin in regulating $\text{Ca}^{2+}$ release

Recent experimental studies have shown that calsequestrin (CSQ), a native SR protein plays a significant role in regulating the CICR process (Beard et al., 2005; Gyorke et al., 2004; Kubalova et al., 2004; Terentyev et al., 2003). CSQ primarily serves as the main  $\text{Ca}^{2+}$  buffer in the SR. It allows for a large amount of  $\text{Ca}^{2+}$  which is required for contraction to be stored inside the cell while maintaining a low level of free  $\text{Ca}^{2+}$  during rest. In addition, CSQ has also been shown to serve as a luminal SR  $\text{Ca}^{2+}$  sensor for RyRs by interacting with other intrinsic SR membrane proteins, Triadin-1 and Junctin. When the SR content is low, CSQ inhibits the RyR channels by strong interaction with Triadin-1 and Junctin. Upon elevation of the SR  $\text{Ca}^{2+}$ , this inhibition is relieved as  $\text{Ca}^{2+}$  binding sites on CSQ become increasingly occupied thus minimizing the interaction with the Triadin-1/Junctin complex (Gyorke et al., 2004).

Mutations of the cardiac CSQ gene, *CASQ2*, have been reported to lead to a variant of catecholaminergic polymorphic ventricular tachycardia (CPVT), a class of hereditary ventricular arrhythmias which may lead to sudden death under  $\beta$ -adrenergic stimulation during stress or exercise (Lahat et al., 2001; Terentyev et al., 2006; Viatchenko-Karpinski et al., 2004). A missense mutation has been suggested to affect CSQ buffering capacity through disruptions in

$\text{Ca}^{2+}$  binding (Lahat et al., 2001; Viatchenko-Karpinski et al., 2004) and another mutation is thought to cause an impairment in the RyR–CSQ interaction (Terentyev et al., 2006). These mutations are thought to promote a calcium overload situation which can induce spontaneous calcium releases and oscillations. However, the precise mechanisms for how these mutations lead to whole-heart events, namely catecholamine-induced arrhythmias, remain unclear.

Experimental studies at the single cell level have further elucidated how CSQ modulates the CICR process through its buffering capacity and its role as the luminal sensor for the RyR channel (Kubalova et al., 2004; Terentyev et al., 2003). Using adenovirus mediated gene transfection, the authors were able to change the level of CSQ expressed inside isolated rat myocytes and show how these changes affect the basic properties of the  $\text{Ca}^{2+}$  release process. A two to three fold increase in CSQ expression causes an increase in the magnitude and duration of calcium release from a CRU (calcium spark) and a reduction in the spontaneous spark frequency. Meanwhile, reducing the CSQ expression to 30–70% of the normal level has the opposite effect: calcium spark magnitude and duration are depressed while the occurrence of spontaneous sparks increases (Terentyev et al., 2003). Generation of spontaneous calcium waves has been studied using permeabilized myocytes where the cytosolic  $\text{Ca}^{2+}$  concentration can be controlled and increased (Kubalova et al., 2004). Similar to the observation for  $\text{Ca}^{2+}$  sparks, higher CSQ expression increases both the wave period and amplitude (obtained by averaging the total  $\text{Ca}^{2+}$  dye fluorescence signal from the entire cell). In contrast, lower CSQ expression decreases the period and amplitude of calcium waves. However, CSQ expression does not appear to change the propagation velocity of calcium waves (Kubalova et al., 2004).

In this paper, we adapt the methodology proposed by Hinch to derive a two-state stochastic process description of a CRU that includes the effects of RyR–CSQ interactions. We then use this model to study the effect of calsequestrin (CSQ) in regulating the local control process. We separately consider the effect of CSQ as a buffer alone, and as a luminal sensor to RyR. We look more closely at how luminal sensing changes the calcium release process by comparing the profiles of calcium release and spark generation obtained from a model that takes into account luminal sensing to those from a model that only includes the buffering effect. From our comparison, we show that different results from an existing experimental study (Kubalova et al., 2004) can only be explained by luminal sensing effects.

Recent studies by Stevens et al. (2009) showed that whole-cell oscillation is observed under high cytoplasmic calcium concentration. By tracking the level of calcium inside the SR, the authors found that increasing cytoplasmic calcium in permeabilized myocytes resulted in spontaneous calcium oscillations due to periodic closing and opening of the RyR channels. Motivated by their finding, we study the effect of increasing the cytoplasmic calcium level in our CRU model. By analyzing the model, we show how the onset of oscillation is modulated by the CSQ level.

The outline of this paper is as follows. First, we derive a simplified stochastic  $\text{Ca}^{2+}$  model. We begin by giving the mathematical description of a CRU, similar to the one given by Hinch (2004), Hinch and Chapman (2005). By making use of mean first exit time calculations from the master equations, we are able to approximate the behavior of the RyR cluster within a CRU as a two-state process without making the assumption that the channel cluster acts as one mega-channel, a common assumption in the existing literature (Hinch et al., 2004; Williams et al., 2007). We then use the reduced model to study changes in calcium release and oscillation under modulation of CSQ expression levels. Finally, we end the paper by summarizing our findings and addressing the limitations of our models.

## 2. Mathematical model of a calcium release unit

### 2.1. Calcium concentrations

Consider a CRU as illustrated in Fig. 1. Suppose that there are  $N$  RyRs within the unit. The rate of change of the amount of calcium within a diadic space of volume  $v_{ds}$  is given by the equation,

$$v_{ds} \frac{dc_{ds}}{dt} = \sum_{i=1}^N X_i g_r (c_{jsr} - c_{ds}) - g_d (c_{ds} - c_{myo}), \quad (1)$$

where  $c_{ds}$  is the calcium concentration in the diadic space. The first term on the right-hand side corresponds to  $Ca^{2+}$  flux through RyRs, where  $X_i$  is a random variable taking on the value of 0 or 1 depending on whether the  $i$ -th RyR receptor is closed or open, respectively. The junctional SR concentration is denoted by  $c_{jsr}$ , and  $g_r$  is the single channel RyR permeability. The second term describes the diffusive flux between the diadic space and the bulk myoplasmic space with calcium concentration,  $c_{myo}$ , and flux rate  $g_d$ . A term corresponding to the LCC influx can also be added into the equation but we omit this term here, as we wish to consider only the process of spontaneous calcium release.

Similarly, a differential equation describing the calcium concentration in the JSR,  $c_{jsr}$ , can be written as

$$v_{jsr} \frac{dc_{jsr}}{dt} = \beta_{jsr} \left( - \sum_{i=1}^N X_i g_r (c_{jsr} - c_{ds}) + g_{tr} (c_{nsr} - c_{jsr}) \right), \quad (2)$$

where  $g_{tr}$  is the diffusion rate between the NSR compartment, with concentration  $c_{nsr}$ , to the JSR. Buffering in the JSR occurs due to the presence of calsequestrin with fast calcium binding kinetics (Beltran et al., 2006; Swietach et al., 2008; Shannon et al., 2004). It is thus accounted for in this model using a rapid buffering approximation (Keener and Sneyd, 1998),

$$\beta_{jsr} = \left( 1 + \frac{B_q K_q}{(K_q + c_{jsr})^2} \right)^{-1}. \quad (3)$$

$B_q$  is the total CSQ buffer concentration and  $K_q$  is the CSQ- $Ca^{2+}$  disassociation constant. The level of free CSQ buffer,  $q$ , can also be written as an instantaneous function of the free JSR calcium,  $c_{jsr}$ ,

$$q(c_{jsr}) = \frac{B_q K_q}{K_q + c_{jsr}}. \quad (4)$$

In the equations for  $c_{ds}$  above, there is no buffering term. This is a simplifying assumption which can be modified as needed. It should be noted that the significance of calcium buffering in the diadic space is unclear. The volume of the diadic space is so small that the rate at which  $Ca^{2+}$  binds to a cytosolic buffer is much slower than the rate at which  $c_{ds}$  equilibrates to  $c_{myo}$ . Moreover, since the CRU only represents a small portion of the cell with a relatively small volume, we assume that calcium concentrations

in the JSR and the diadic space are spatially homogeneous. The parameter values used for the model can be found in Table 1.

The timescale over which calcium concentration in the diadic space equilibrates with the concentration in the bulk myoplasm is  $\tau_{ds} = v_{ds}/g_d$ . This has been estimated to be on the order of a few  $\mu s$  which is much quicker than the timescale of other processes, such as JSR refilling and channel gating, which occur on the order of ms (Bers, 1991; Hinch, 2004; Hinch et al., 2004; Sobie et al., 2002). Thus, using a quasi-equilibrium approximation, the diadic space concentration,  $c_{ds}$ , can be written as a function of the number of open RyRs,  $n$ ,

$$c_{ds}(n) = c_{myo} + n \frac{g_r}{g_d} c_{jsr}. \quad (5)$$

In deriving this relationship, we also take  $g_r/g_d \ll 1$  as the single channel permeability of RyR is much smaller than the rate of diffusion between the diadic space and the bulk myoplasm. The derivation of these approximations which includes non-dimensionalization steps in order to find small parameters, can be found in Hinch (2004).

### 2.2. Ryanodine receptor and calsequestrin interaction

To study how CSQ modulates the calcium release process in the CRU, we build a Markov model for RyR activity that accounts for the channel interaction with CSQ. The full model is given in Fig. 2. RyR activity is assumed to be modulated by cytosolic  $Ca^{2+}$  concentration. When calcium is low, the channel is in the closed state  $C_1$ . As the calcium concentration increases, four  $Ca^{2+}$  ions can bind to the channel bringing it to the  $C_2$  state and a transition to the conducting state  $O$  can then be made. To account for CSQ interaction, we assume that free CSQ with concentration  $q$ , can bind and unbind to the RyR channel causing it to be in the  $B$  and  $U$  states, respectively. It is found that increasing luminal  $Ca^{2+}$  increases channel activity by increasing the number of openings rather than prolonging the open time duration (Gyorke and Gyorke, 1998). Based on this, we assume that CSQ affects the RyR activity by changing its open rate. When a CSQ molecule is bound, the channel is inhibited so the open rate  $k_2$  is multiplied by a constant  $a$  which is less than one. To preserve detailed-balance, we multiply the transition from  $O_U$  to  $O_B$  by  $a$  as well.

This six-state model can be reduced to a two-state model by assuming that calcium and CSQ binding and unbinding are fast so that these transitions can be assumed to be in quasi-equilibrium. The resulting reduction gives

$$C \xrightleftharpoons[A]{A(c,q)} O, \quad (6)$$

where

$$A(c,q) = k_2 \frac{c^4}{K_r^4 + c^4} \left( \frac{K_3 + aq}{K_3 + q} \right), \quad (7)$$

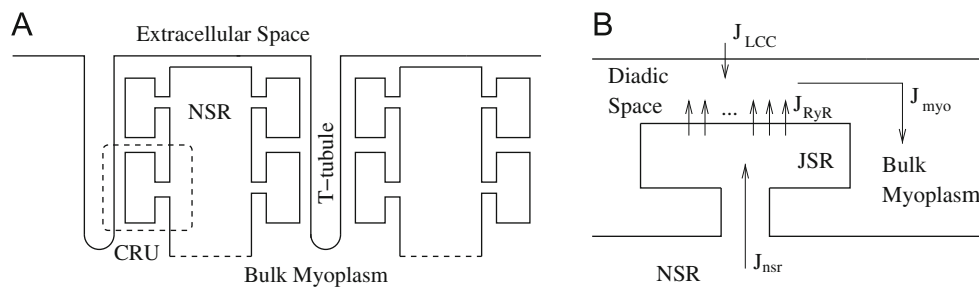


Fig. 1. Diagram of calcium release units. (A) Illustration of a cell composed of a number of CRUs. (B) Each unit has a separate diadic space and a junctional SR compartment and is coupled to its neighbors through the bulk myoplasmic space and the network SR.

**Table 1**  
List of parameters values for the CRU model.

Parameter	Definition	Value	Source
$v_{ds}$	Diadic space volume	$10^{-4} \mu\text{m}^3$	[1,2]
$v_{jsr}$	JSR volume	$0.01 \mu\text{m}^3$	[1,2]
$c_{myo}$	Bulk myoplasmic $[\text{Ca}^{2+}]$	$0.1 \mu\text{M}$	[1,2]
$c_{nsr}$	Network SR $[\text{Ca}^{2+}]$	$1000 \mu\text{M}$	[1,2]
$g_d$	Flux rate between the myoplasm and the diadic space	$0.286 \mu\text{m}^3 \text{ms}^{-1}$	[1,2]
$g_{tr}$	Flux rate between the JSR and the NSR	$0.001 \mu\text{m}^3 \text{ms}^{-1}$	[1,2]
$N$	Number of RyRs	40	[1]
$g_r$	Permeability of a single RyR	$0.01/N \mu\text{m}^3 \text{ms}^{-1}$	[1]
$B$	RyR closing rate	$2 \text{ms}^{-1}$	Simplified [1]
$k_2$	Maximum RyR open rate	$12 \text{ms}^{-1}$	Simplified [1]
$K_R$	RyR- $\text{Ca}^{2+}$ dissociation constant	$6 \mu\text{M}$	Simplified [1]
$m$	Number of $\text{Ca}^{2+}$ binding sites on RyR	4	[1]
$a$	Scaling for RyR open rate when CSQ is bound	0.25	Chosen less than 1
$K_3$	RyR-CSQ dissociation constant	$2.0 \text{mM}$	[3] <sup>a</sup>
$B_q$	Total [CSQ] in the JSR	$2.7 \text{mM}$	[4]
$K_q$	CSQ- $\text{Ca}^{2+}$ dissociation constant	$0.65 \text{mM}$	[5]

[1]: Hinch (2004), [2]: Sobie et al. (2002), [3]: Beard et al. (2005), [4]: Shannon et al. (2000), [5]: Terentyev et al. (2002).

<sup>a</sup> The value of  $K_3$  is estimated such that when  $c_{jsr}$  is above 4 mM, the fraction of CSQ-bound RyR is less than 10%, reflecting the observation that luminal  $[\text{Ca}^{2+}] \geq 4 \text{mM}$  dissociates CSQ from the junctional face membrane (Beard et al., 2005).

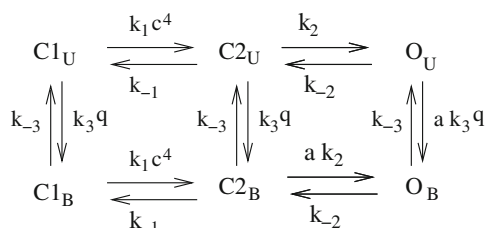


**Fig. 2.** Markov model for RyR–CSQ interaction.

with  $K_r^4 = k_{-1}/k_1$ ,  $K_3 = k_{-3}/k_3$ , and  $B = k_{-2}$ . Note that when the luminal sensing parameter  $a$  is set to one or without any free CSQ,  $q=0$ , the open rate reduces to the standard calcium-dependent activation form. Parameter values for this RyR model are given in Table 1.

Note that a refractory or inactivated state is not included in this RyR model. Results from past studies suggest that inactivation by cytosolic calcium does not play a significant role in controlling calcium release in cardiac cells (Terentyev et al., 2003). Instead, when CSQ is bound to RyRs, the channel becomes less active but it can reopen if the diadic space calcium concentration increases. Fig. 3A shows the dependence of free CSQ on  $c_{jsr}$  as given in Eq. (4). As  $c_{jsr}$  decreases, the level of free CSQ that can bind to the RyR channel increases. CSQ binding impedes the activity of RyRs by decreasing the open rate and increasing the threshold for activation. This is shown in the Fig. 3B where  $a(c_{ds})$  is plotted for varying  $c_{jsr}$  values.

### 3. $\text{Ca}^{2+}$ release unit as a two-state stochastic process

#### 3.1. Deterministic limit

Before analyzing the stochastic behavior of the model, we first study it in its deterministic limit. In the limit that the total number of RyRs,  $N$ , goes to infinity, we can use the law of large numbers to replace the random variable for the number of open channels,  $n$ , at any given time, by its expected value. Switching from a discrete integer-valued  $n$  to the continuous fraction  $x=n/N$  of the number of open channels, the ordinary differential equation

for the mean can be written by applying mass action principle on (6),

$$\frac{dx}{dt} = A(c_{ds}(x), q(c_{jsr}))(1-x) - Bx. \quad (8)$$

The function  $c_{ds}(x)$  is similar to (5),

$$c_{ds} = c_{myo} + \frac{Ng_r}{g_d} x c_{jsr}. \quad (9)$$

Note that in Table 1, the maximum release rate  $Ng_r$  is a fixed quantity even though the deterministic  $N \rightarrow \infty$  limit is taken.

Following the quasi-equilibrium approximations steps used to obtain (5), the dynamics of  $c_{jsr}$  are given by

$$v_{jsr} \frac{dc_{jsr}}{dt} = \beta_{jsr} (-Ng_r x c_{jsr} + g_{tr}(c_{nsr} - c_{jsr})). \quad (10)$$

The two coupled ordinary differential equations (8) and (10) form a fast–slow excitable system. Compared to  $x(t)$ ,  $c_{jsr}(t)$  changes on a slower timescale. Fig. 4 illustrates how the two variables change over time once a spark is initiated. On Fig. 4A, the time course for  $x(t)$  and  $c_{jsr}(t)$  during the spark are plotted. Fig. 4B shows the phase plane of the system with the sample trajectory plotted. We note the similarity of this excitable CRU system with cubic-like nullcline, to the Fitzhugh Nagumo model for action potentials (Keener and Sneyd, 1998).

In this deterministic limit, spontaneous spark generation is not possible as the equilibrium solution corresponding to the rest state is stable. Deterministic sparks can be generated only by perturbing sufficiently away from the stable rest state such as by starting from a non-equilibrium initial condition, as done for this particular trajectory, or by adding an input term to  $c_{ds}(x)$ . Once a spark is generated, the trajectory quickly moves to the right branch of the  $x$ -nullcline and moves down the nullcline until it falls off. Calcium release terminates at this point. Following that, the trajectory quickly switches to the left branch of the nullcline and moves up towards the equilibrium point as  $c_{jsr}$  recovers through refilling by the NSR. It is important to note that in the deterministic system, termination occurs at one particular  $c_{jsr}$  value near the location of the minimum of the  $x$ -nullcline. Only after  $c_{jsr}$  drops to this critical value does calcium release terminate.

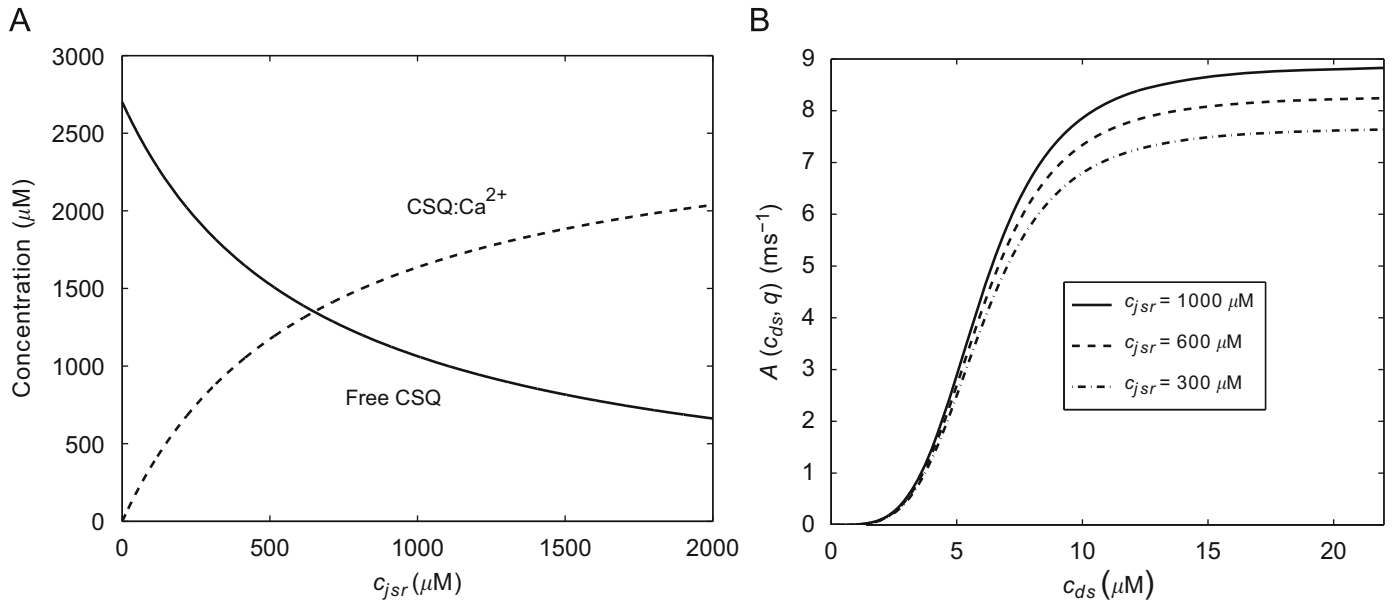


**Fig. 3.** RyR and CSQ dependence of calcium: (A) the free CSQ and the CSQ:Ca<sup>2+</sup> complex concentrations as functions of the free JSR Ca<sup>2+</sup> concentration and (B) plot of RyR open rate for varying values of JSR Ca<sup>2+</sup>.

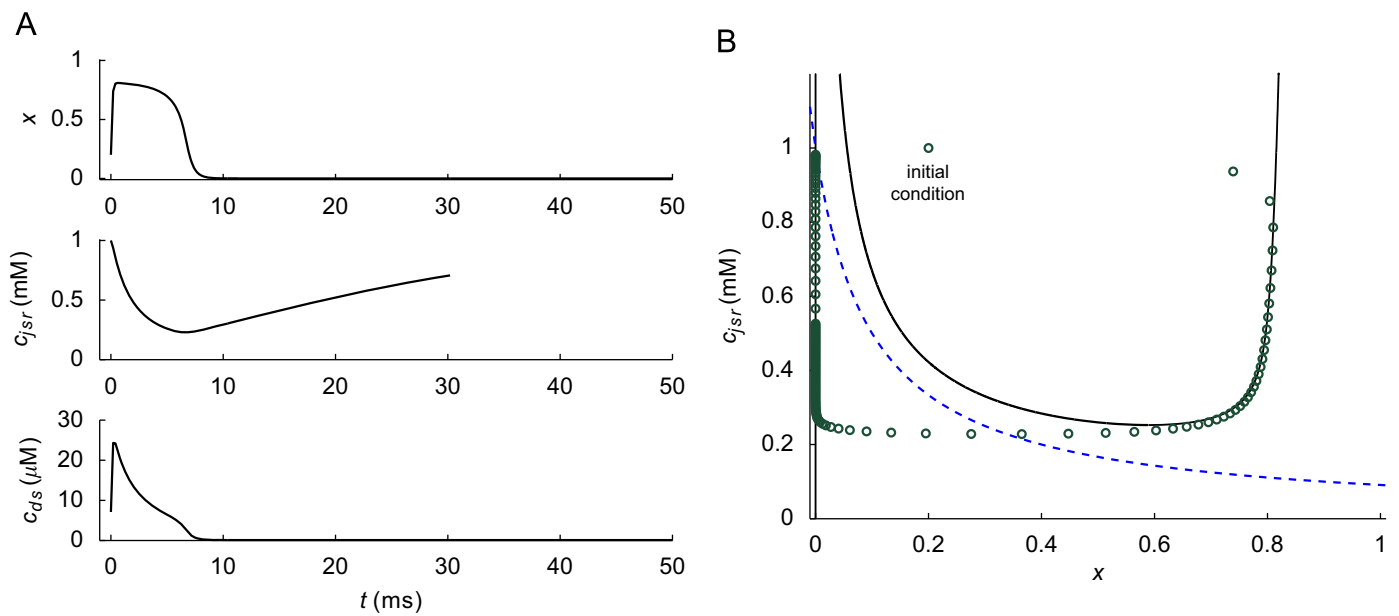
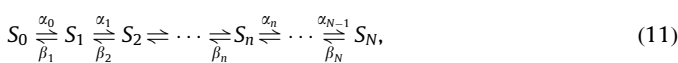


**Fig. 4.** CRU dynamics during a simulated spark: (A) time course of  $x(t)$  and  $c_{jsr}(t)$  with initial conditions  $x(0)=0.2$  and  $c_{jsr}(0)=1000 \mu\text{M}$ . The diadic space concentration,  $c_{ds}$ , is obtained from Eq. (9) and (B) phase plane diagram with sample points of the trajectory plotted in dots. Solid lines indicate the  $x$ -nullcline and dashed line gives the  $c_{jsr}$ -nullcline.

### 3.2. Stochastic CRU

To consider spontaneous spark generation and the possibility of spark termination before the critical  $c_{jsr}$  is reached, single channel activities must be tracked. The behavior of a cluster of  $N$  RyRs in the CRU can be described by the birth–death process,



where  $S_n$  is the state with  $n$  RyR channels open. The rates are

$$\alpha_n = (N-n)A(c_{ds}(n), q(c_{jsr})) \quad \text{and} \quad \beta_n = nB. \quad (12)$$

The forward rate  $\alpha_n$  indicates that there are  $N-n$  channels available to open where each can open at a rate  $A(c_{ds}(n), q(c_{jsr}))$  as

given by (7). Similarly,  $\beta_n$  accounts for the fact that there are  $n$  open channels that can each close at the rate  $B$ . The corresponding master equation for this process is listed in Appendix A.

In Fig. 5, we show a realization obtained by simulating the full stochastic system consisting of the birth process (11) above and Eq. (2) for  $c_{jsr}$  dynamics. Starting from the deterministic equilibrium point, a spontaneous spark is generated after a long wait time. During this time, small fluctuations in the number of open channels can occur. However, a full CRU release is not generated until a threshold is reached. This threshold lies close to the middle branch of the  $x$ -nullcline of the deterministic system or the local minimum between the two maxima of the stationary distribution of the birth–death process (see Appendix A). Once the threshold is reached, the number of open channels increases

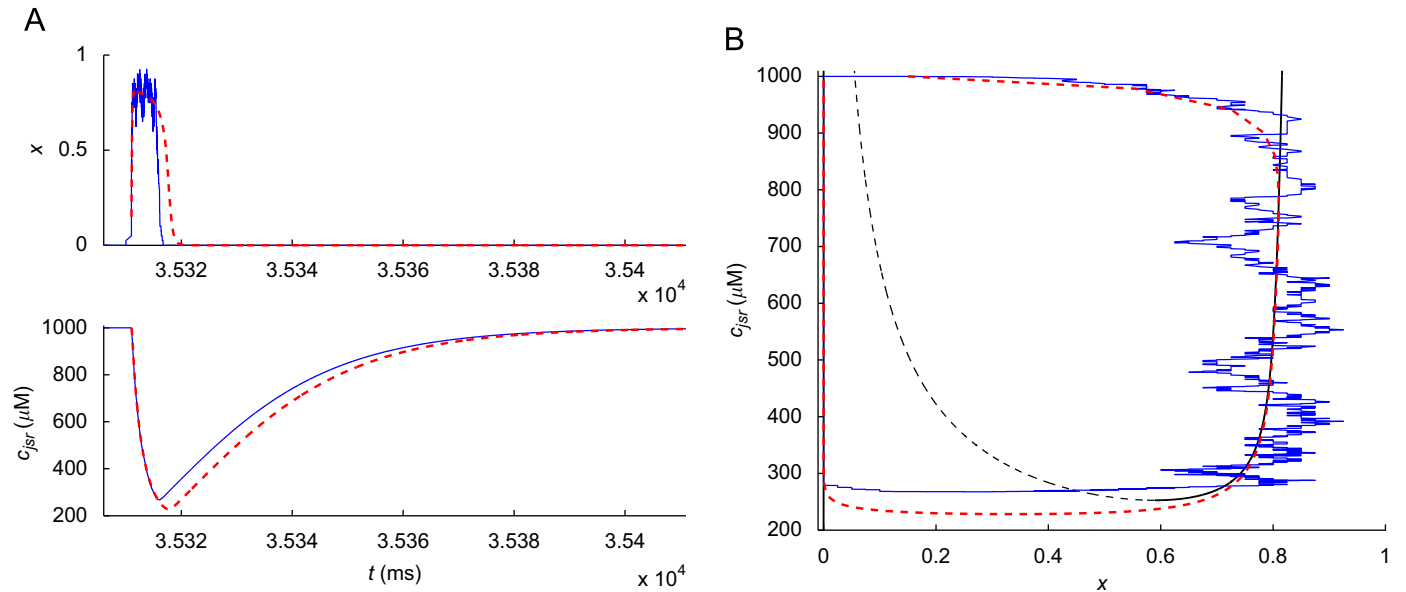


**Fig. 5.** Simulation of the stochastic CRU system consisting of the birth death process (11) and Eq. (2) for  $c_{jsr}$  dynamics: (A) time course of  $x(t)$  and  $c_{jsr}(t)$ . For comparison, the deterministic trajectory is shown in a dashed line and (B) the stochastic realization plotted on the phase plane showing fluctuations about the nullcline during calcium release. In addition, release can possibly terminate before the critical JSR value is reached as shown for this particular realization.

quickly and the stochastic trajectory fluctuates about the right branch of the deterministic  $x$ -nullcline as shown in Fig. 5. As the  $c_{jsr}$  value drops, the likelihood of release to terminate increases. For this particular realization, calcium release terminates before the deterministic critical JSR level is reached.

Having shown the result obtained from simulating the full stochastic CRU description, we outline below the derivation of a reduced stochastic description. This reduction is essential in particular as a spontaneous CRU release is rare with a long waiting time for occurrence. Thus, relying on full simulation to obtain an accurate statistics of CRU release is not practical, if not unfeasible.

1. In the deterministic limit discussed above, a CRU behaves as a fast-slow excitable system. The fraction of open channels  $x(t)$  acts as a fast variable while the JSR calcium  $c_{jsr}$  has much slower dynamics. This timescale separation is illustrated clearly in Fig. 4A. More specifically, the timescale for  $c_{jsr}$  to equilibrate with the bulk network SR  $c_{nsr}$  is given by  $v_{jsr}/\beta_{jsr} \cdot g_{tr} = 15\text{--}30$  ms, while the timescale for  $x$  to decay back to the zero release state is  $1/B = 2$  ms. Based on this, we can make another quasi-equilibrium approximation, namely that  $x$  changes instantaneously given a  $c_{jsr}$  value. In essence, we restrict  $x$  to the left and right branches of the nullcline given in Fig. 4B. We denote the left branch, representing the low conductance state of the CRU, as  $x_0(c_{jsr})$  and the right branch, corresponding to a high conductance state, as  $x_1(c_{jsr})$ . The JSR calcium,  $c_{jsr}$ , is now the only dynamic variable tracked and is given by the equation

$$v_{jsr} \frac{dc_{jsr}}{dt} = \beta_{jsr} (-N g_{tr} x_i(c_{jsr}) c_{jsr} + g_{tr} (c_{nsr} - c_{jsr})), \quad (13)$$

with  $i=0$  or  $1$ .

2. Unlike in the deterministic case, we allow  $x$  to switch between the two branches stochastically. Thus, spontaneous spark generation and early spark termination are possible. The switching rates can be obtained by considering a birth–death process for channel openings and solving the corresponding mean first passage time problems (see Appendix B for details of the derivation). Then, the fraction of open channels,  $x$ , can be

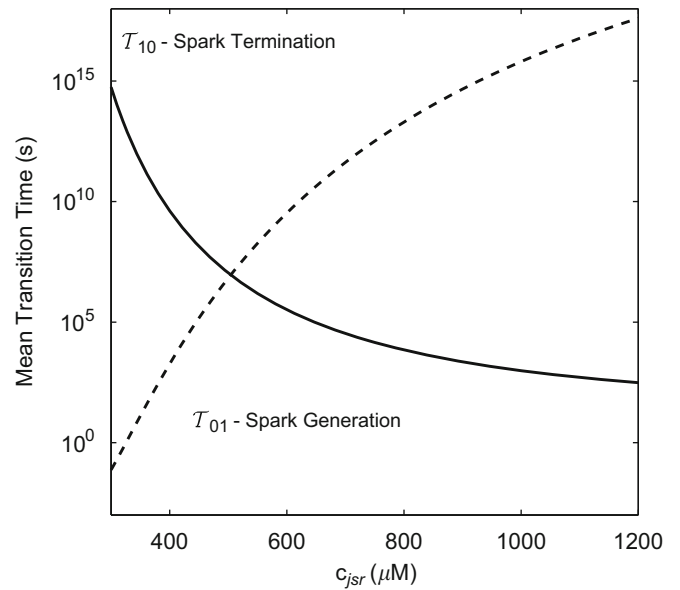


**Fig. 6.** Mean transition times,  $T_{01}$  and  $T_{10}$ , as functions of  $c_{jsr}$ .

written as the following two-state stochastic process:



where the rates are the inverse of the mean first passage times whose analytic formulas are given in Eqs. (B.6) and (B.8) in Appendix B,

$$k_{on}(c_{jsr}) = \frac{1}{T_{01}(c_{jsr})} \quad \text{and} \quad k_{off}(c_{jsr}) = \frac{1}{T_{10}(c_{jsr})}. \quad (15)$$

The transition between  $x_0$  and  $x_1$  can occur at any  $c_{jsr}$  value, albeit at highly variable rates, and is not restricted to any critical points on the deterministic nullcline. The dependence of the transition rates on JSR level are shown in Fig. 6 where  $T_{01}$  and  $T_{10}$  are plotted as functions of  $c_{jsr}$ . Both mean

transition times are modulated by  $c_{jsr}$  and can change by orders of magnitude as the JSR concentration varies within a physiological range.

To summarize, we have thus far reduced the CRU model to a two-state stochastic process described by Eqs. (13) and (14). The transition rates between the two states can be computed analytically and are dependent on the JSR  $Ca^{2+}$  concentration as shown in Fig. 6. Unlike the full model which consists of  $N$  random variables describing each individual RyR, a simulation of our model only requires a single random variable to be tracked. This reduction still accounts for multiple channel activity and we do not treat all RyRs in the CRU as a single mega-channel as in Williams et al. (2007), where the number of open channels in a CRU is strictly either zero or a fixed positive value. In our model,  $x_0$  and  $x_1$  are not of constant value but rather are dependent on  $c_{jsr}$ . Although for a wide range of  $c_{jsr}$  value,  $x_0$  and  $x_1$  appears relatively constant, their value can change significantly in some critical range of JSR concentration. For example near the deterministic termination point, the  $x$ -nullcline changes sharply as  $c_{jsr}$  varies.

### 3.3. Spark profiles of the two-state CRU model

Spontaneous sparks are rarely observed in healthy cardiac cell, but under a calcium overload condition, the frequency of  $Ca^{2+}$  sparks increases. This can be seen in the plot for  $\mathcal{T}_{01}$  in Fig. 6. As  $c_{jsr}$  increases, the expected time for a spontaneous spark generation decreases. When  $c_{jsr}$  is  $1000 \mu M$ ,  $\mathcal{T}_{01}$  is 970 s. This result can be translated to the whole-cell level which is more experimentally relevant. Conversion to a whole-cell spark rate is obtained by taking the inverse,  $1/\mathcal{T}_{01}$ , and multiplying it by the number of CRUs within a cell which we assume to be 10,000. Then, when the JSR  $Ca^{2+}$  is at  $1000 \mu M$ , the average whole-cell spark rate is 10 sparks per second. Increasing  $c_{jsr}$  to  $1200 \mu M$  approximately triples the spark rate to 30 sparks per second.

$\mathcal{T}_{10}$  is the expected spark termination time if  $c_{jsr}$  value were held fixed throughout release. As can be seen in Fig. 6,  $\mathcal{T}_{10}$  is large and does not decrease to a level that is physiologically relevant until  $c_{jsr}$  is very low. Thus, to study the actual spark termination process, the dynamics of  $c_{jsr}$  needs to be taken into account. We define the spark termination time as the time at which switching from  $x_1$  to  $x_0$  occurs. Suppose the CRU is in a releasing state  $x_1$ . Let  $t_{term}$  be the random variable describing the time at which termination of release occurs. The probability of termination per unit time is  $1/\mathcal{T}_{10}(c_{jsr}(t))$ . Defining  $P(t)$  as the cumulative

distribution function for the termination time  $t_{term}$ , i.e.,  $P(t) = \Pr\{t_{term} \leq t\}$ , we can then write,

$$\frac{dP}{dt} = \frac{1}{\mathcal{T}_{10}(c_{jsr}(t))} (1 - P(t)). \quad (16)$$

Solving this equation, we get

$$P(t) = 1 - \exp\left(-\int_0^t \frac{1}{\mathcal{T}_{10}(c_{jsr}(s))} ds\right). \quad (17)$$

The probability density function can be obtained by differentiating  $P(t)$ ,

$$p(t) = \frac{1}{\mathcal{T}_{10}(c_{jsr}(t))} \exp\left(-\int_0^t \frac{1}{\mathcal{T}_{10}(c_{jsr}(s))} ds\right). \quad (18)$$

Spark termination results predicted from the deterministic and stochastic CRU models are shown in Fig. 7. The probability density function and the cumulative distribution function are plotted in Fig. 7A and B, respectively, while the result obtained from simulating the deterministic system (8) and (10) is shown in Fig. 7C. We define the deterministic termination time as the time at which  $c_{jsr}$  reaches its minimum, i.e. the time before the refilling process begins. From the mean and variance calculated using the probability distribution function, the spark duration predicted from the stochastic reduction is  $7.3 \pm 2.4$  s. This average value is slightly higher than 6.6 s, the value obtained from the deterministic model. However, the peak of the probability distribution function lies below the time deterministic spark termination time. Moreover, the cumulative distribution function shows that the probability that a spark is terminated before the critical  $c_{jsr}$  value is approximately 50%. Note that in obtaining the distribution and density functions, we use the  $c_{jsr}$  value obtained from Eq. (13), however, once the critical  $c_{jsr}$  value is reached, we no longer allow  $c_{jsr}$  to change. The profile for the JSR  $Ca^{2+}$  used is shown in dashed line in Fig. 7C. With this assumption, once the critical value is reached, the spark termination time simply follows an exponential distribution with a constant rate. As time progresses, the cumulative distribution function tends to one.

## 4. Results

### 4.1. Fundamental effects of luminal sensing

We first study the intrinsic effects of luminal sensing by comparing results obtained from our RyR model with  $a=1$  and

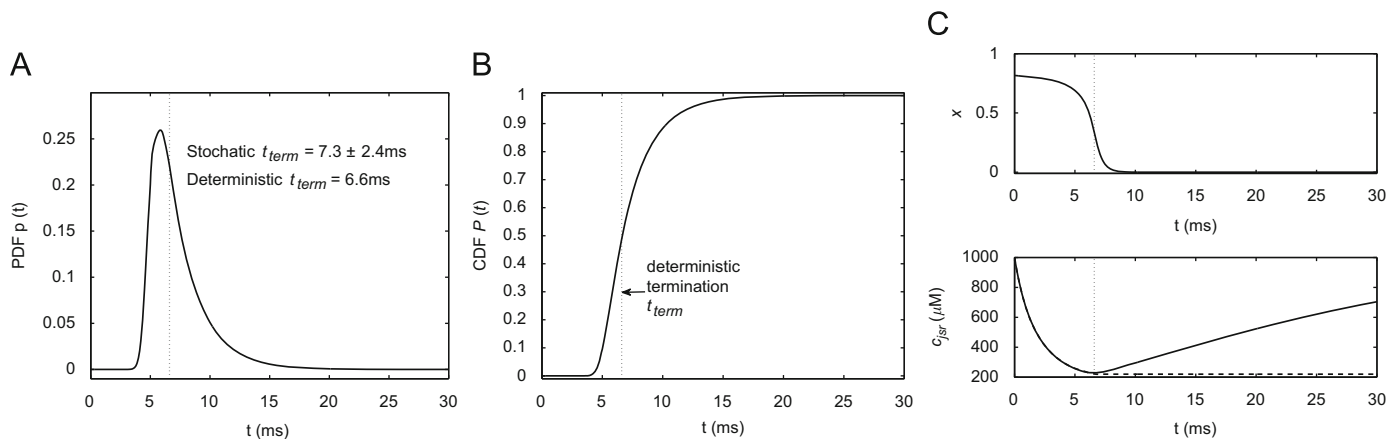


**Fig. 7.** Deterministic and stochastic termination of  $Ca^{2+}$  release: (A) probability density  $p(t)$  for spark termination time; (B) cumulative distribution  $P(t)$  for spark termination time; and (C) deterministic spark termination obtained by simulating Eqs. (8) and (10) with initial conditions  $c_{jsr}(0) = 1000 \mu M$  and  $x(0) = x_1(c_{jsr}(0))$ . The  $c_{jsr}$  profile used to obtain  $p(t)$  and  $P(t)$  in (A) and (B) are shown in dashed line at the bottom panel of (C). The dotted lines in (A), (B), and (C) indicate the deterministic spark termination time which occurs when  $c_{jsr}(t)$  reaches its minimum value.

0.25. When  $a=1$ , the dependence of the RyR open rate  $A(c, q)$  on the calsequestrin level (hence JSR concentration) drops out as shown in Eq. (7). Thus, in this case, calsequestrin simply serves as a buffer in the SR. As the value of  $a$  decreases below one, the luminal sensing effect becomes more important. Basic results obtained from these two cases are shown in Fig. 8. In Fig. 8A, the mean exit time for spark generation,  $T_{01}$ , and termination,  $T_{10}$ , are first computed under varying JSR  $\text{Ca}^{2+}$  load. When  $c_{\text{jsr}}$  is high, the mean spontaneous spark time generation,  $T_{01}$ , for the two models are of the same order. However, as  $c_{\text{jsr}}$  starts to drop, the  $T_{01}$  value obtained from the RyR-CSQ model is higher reflecting RyR luminal sensing. When the JSR load is low, the interaction between RyRs and CSQ is strong, so the channel becomes desensitized and spontaneous spark generation becomes less

likely. The expected time for spark termination,  $T_{10}$ , obtained when luminal sensing is included, is lower compared to the one obtained when  $a=1$ . As a result, the average spark duration is shorter when  $a < 1$ . This is also confirmed by the deterministic CRU simulation of a spark given in Fig. 8B. Thus, termination of release occurs earlier and at a slightly higher JSR load when  $a < 1$ .

#### 4.2. Effects of calsequestrin amount on calcium release profiles

We now study how calsequestrin modulates calcium release by changing the total amount of calsequestrin in the system,  $B_q$ . Throughout our analysis, we specifically consider three different levels of CSQ expression: a normal level, a 30% decrease, and a

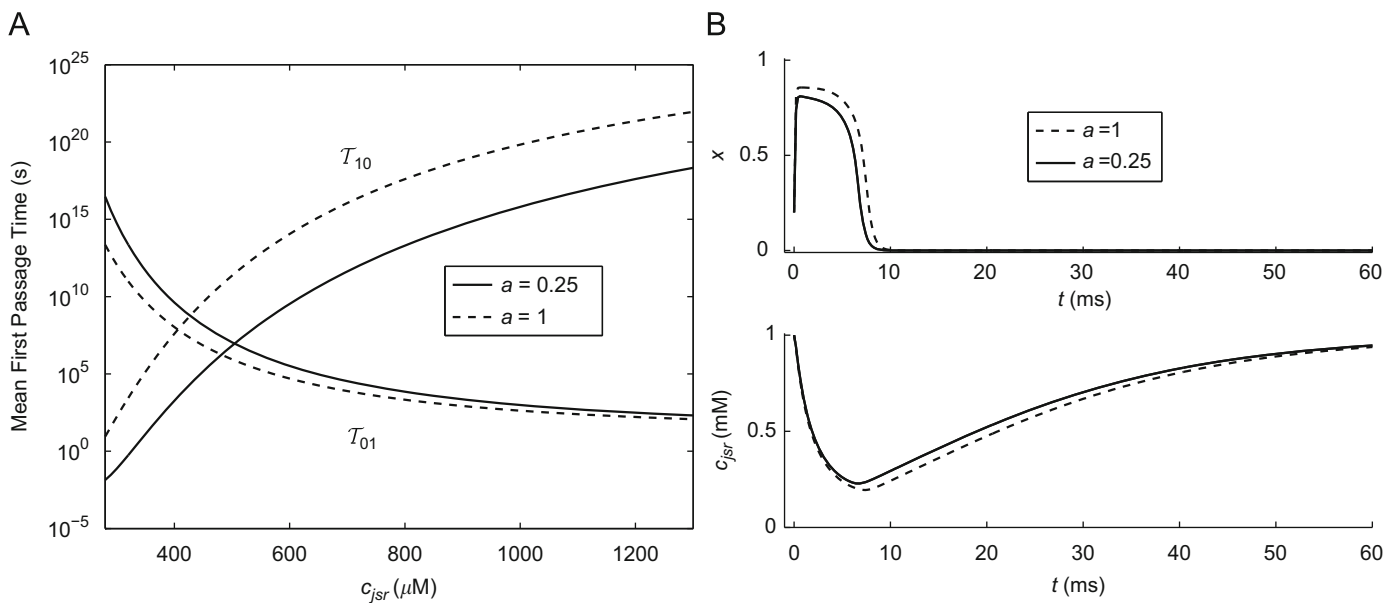


**Fig. 8.** Comparisons of results from the RyR-CSQ model when the luminal sensing effect is included,  $a < 1$  or when CSQ is treated simply as a buffer,  $a=1$ : (A) comparison of mean transition times,  $T_{01}$  and  $T_{10}$  and (B) deterministic CRU simulations for the two models. When  $a < 1$ , spontaneous spark generation becomes less likely particularly when  $c_{\text{jsr}}$  is lower. As the interaction between RyR and CSQ grows, the channel becomes desensitized so that its open rate drops as reflected in Eq. (7). In addition, spark termination time is also lower for the  $a < 1$  case.

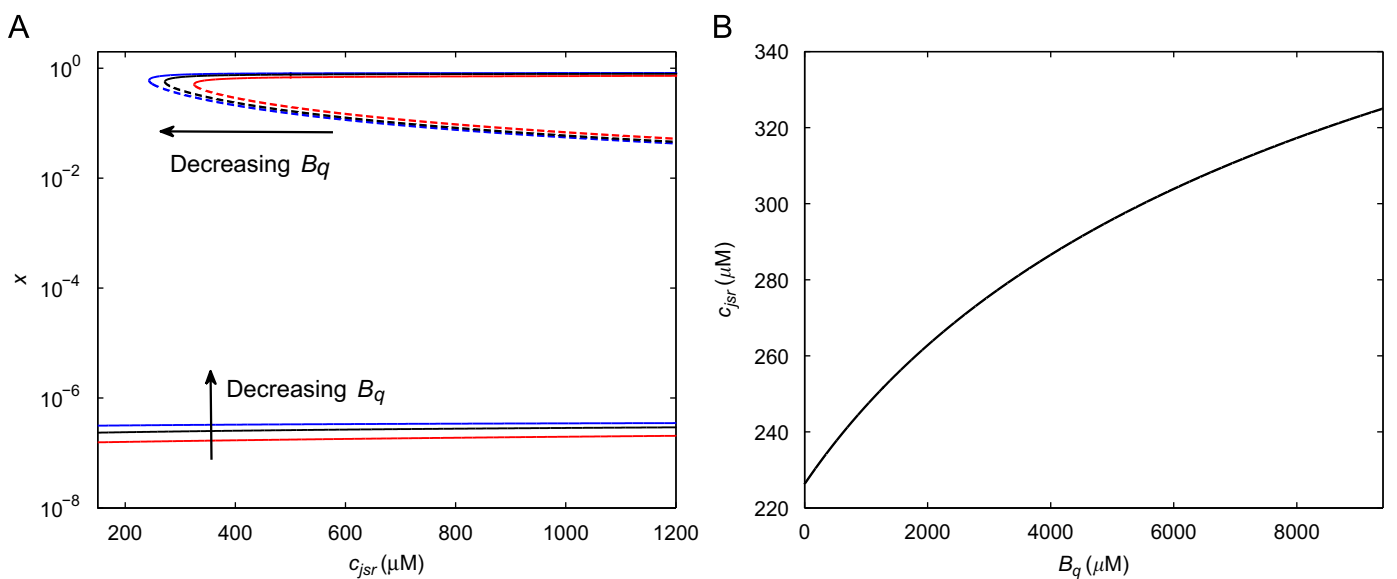


**Fig. 9.** Changes in the bifurcation diagrams under different level of CSQ expressions: (A) steady-state values of  $x$  as a function of  $c_{\text{jsr}}$  and (B) critical  $c_{\text{jsr}}$  value for spark termination as a function of total CSQ concentration,  $B_q$ .

350% increase. These values are specifically chosen so that we can compare our theoretical results to the experimental study by Kubalova et al. (2004). We also assume that changing CSQ expression does not affect the free NSR calcium concentration. As a result, the steady-state value of free JSR calcium concentration remains relatively fixed regardless of the value of  $B_q$ . This assumption is consistent with experimental observations (Kubalova et al., 2004) where CSQ level does not change the free SR calcium level.

We first look at the results obtained using the full model with  $a=0.25$ , when both CSQ buffering and luminal sensing are taken into consideration. The steady-state results from the deterministic system are given in Fig. 9. For the three different values of  $B_q$  considered, the bifurcation diagrams which show the dependence of the nullcline  $dx/dt=0$  (see Eq. (8)) on  $c_{jsr}$ , are shown in Fig. 9A. The limit-point bifurcation where the stable upper branch solution is lost predicts the critical  $c_{jsr}$  value at which calcium release terminates deterministically. When  $B_q$  is decreased, the critical  $c_{jsr}$  value also decreases thus termination of release occurs at a lower  $c_{jsr}$ . This is shown further in Fig. 9B where we plot the critical  $c_{jsr}$  value itself (limit point bifurcation) as a function of  $B_q$ . As the JSR content becomes depleted, the concentration of free CSQ increases thus allowing it to interact with RyR and causing it to become desensitized so that the open rate,  $\alpha(c_{ds}, q)$ , is lowered. Hence, when the total concentration of CSQ,  $B_q$ , is higher, this luminal sensing effect is stronger, causing termination of release to occur at a higher JSR  $Ca^{2+}$ . This occurs despite the fact that the total amount of JSR calcium is higher when  $B_q$  is larger. In contrast, experimental measurements by Kubalova et al. (shown in Figs. 3B and 4B of Kubalova et al., 2004) showed no detectable changes in the amplitude of SR  $Ca^{2+}$  release as CSQ expression levels were varied. It is likely that the changes of JSR level are not detectable since the critical value only varies within  $100 \mu M$  as  $B_q$  is varied by three orders of magnitudes.

To determine spark duration, it is not sufficient to compute the switching time  $\mathcal{T}_{10}$  as the dynamics of  $c_{jsr}$  need to be taken into account. How long a spark lasts is strongly dependent on how fast  $c_{jsr}$  changes with time and the CSQ buffering effect must be taken into account. We use results obtained from solving the deterministic two-variable system to determine how different  $B_q$  values affect the calcium release process. The time courses of various variables during a simulated calcium spark are shown in Fig. 10. From the steady-state analysis, a higher  $B_q$  value causes the release to terminate at a higher  $c_{jsr}$  value. This is observed in Fig. 10A and B. A smaller amount of the CSQ level leads to a higher maximum value for the fraction of open channels,  $x(t)$ , and a lower value for the minimum of  $c_{jsr}(t)$ . The dynamics of  $c_{jsr}$  are also influenced by the scaling factor  $\beta_{jsr}$  given in Eq. (3). As  $B_q$

grows, the value of  $\beta_{jsr}$  decreases so that  $c_{jsr}(t)$  changes more slowly with time. This reflects the fact that when the CSQ level is higher, more  $Ca^{2+}$  can bind to it although the rest level of free  $Ca^{2+}$  inside the SR is not changed. Thus with a higher  $B_q$  value, even though release terminates at a slightly higher free  $c_{jsr}$  value, the time taken to reach this critical value is longer and the amount of  $Ca^{2+}$  released is larger. The calcium transient in the diadic space, can be computed using the quasi-steady-state approximation (9) and is plotted as a function of time in Fig. 10C. The maximum values of the diadic calcium concentration are fairly similar among the three cases though the amplitude is still largest for the lowest  $B_q$  case. However, note that durations of calcium release are more variable. For the highest CSQ expression case, the period of  $Ca^{2+}$  release is longest; thus the total amount of calcium released is larger leading to a larger spark.

To isolate the CSQ buffering effect, we now perform the same computations as above but omitting luminal sensing by setting  $a=1$ . Since the channel open rate  $A(c, q)$  given in Eq. (7) no longer has dependence on the CSQ level, there is no change in the bifurcation diagram (Fig. 9A). The critical  $c_{jsr}$  value at which release terminates is fixed regardless of  $B_q$  value. However, varying the amount of buffer will still change the  $Ca^{2+}$  release duration as well as the length of the refilling period. The amount of CSQ expression alters the  $Ca^{2+}$  spark properties similar to that shown previously in Fig. 10, namely that increasing  $B_q$  lengthens the spark duration. Specific results for the case of  $a=1$  are shown in Fig. 11. The value of  $B_q$  simply determines how fast  $c_{jsr}(t)$  changes with time. Termination of release occurs at the same critical  $c_{jsr}$  value for all three cases. Without any luminal sensing, the buffering effect becomes very prominent. When  $B_q$  is largest, calcium release lasts for a long period of time and is very extended compared to that obtained from the previous  $a < 1$  case. Thus, the release amount is also much larger when  $B_q$  is higher.

Finally, the comparison of release duration as a function of CSQ amount for two different values of  $a$  is shown in Fig. 12A. When  $a=1$ , changing  $B_q$  only affects the buffering factor  $\beta_{jsr}$ . As a result, the release duration is simply a linear function of  $B_q$  since the time-constant  $1/\beta_{jsr}$  for the  $dc_{jsr}/dt$  equation, depends linearly on  $B_q$  (see Eq. (3)). This is no longer the case when  $a < 1$ . For small  $B_q$  values, the release durations for the two cases are similar. In this case, most of the calsequestrin population is calcium bound and does not interact with RyR. However, as  $B_q$  is increased, the effect of luminal sensing becomes more prominent as release duration is much shorter when  $a < 1$ . Although the time-scale over which  $c_{jsr}$  drops still grows longer as  $B_q$  is increased, this effect is also counteracted by luminal sensing. First, calcium release terminates at a higher  $c_{jsr}$  as shown previously in Fig. 9B. In addition, as

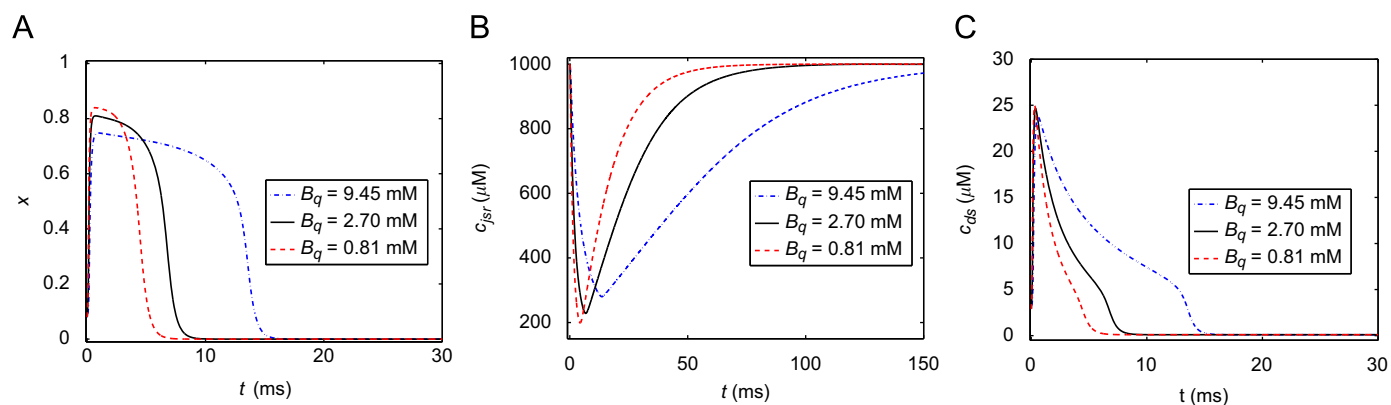
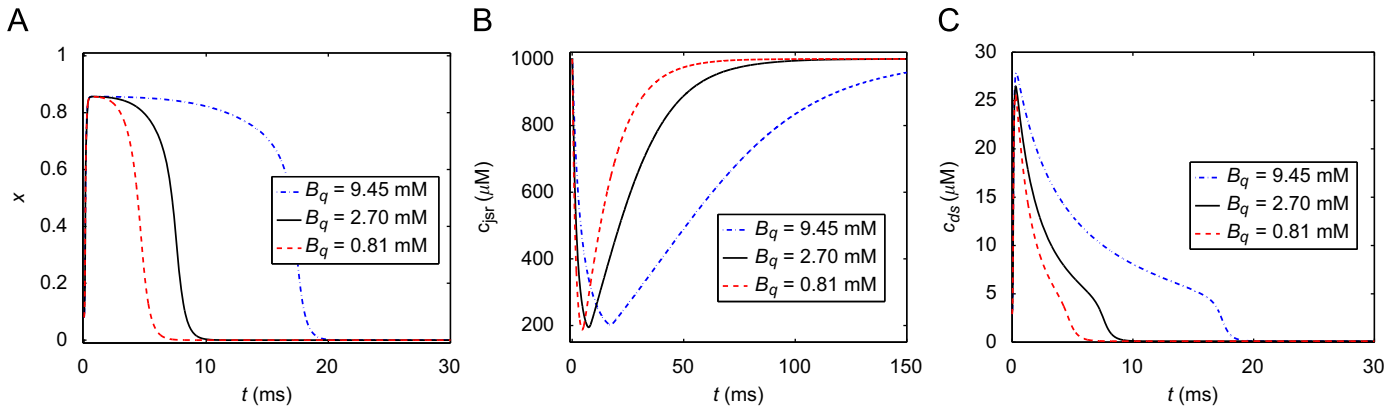
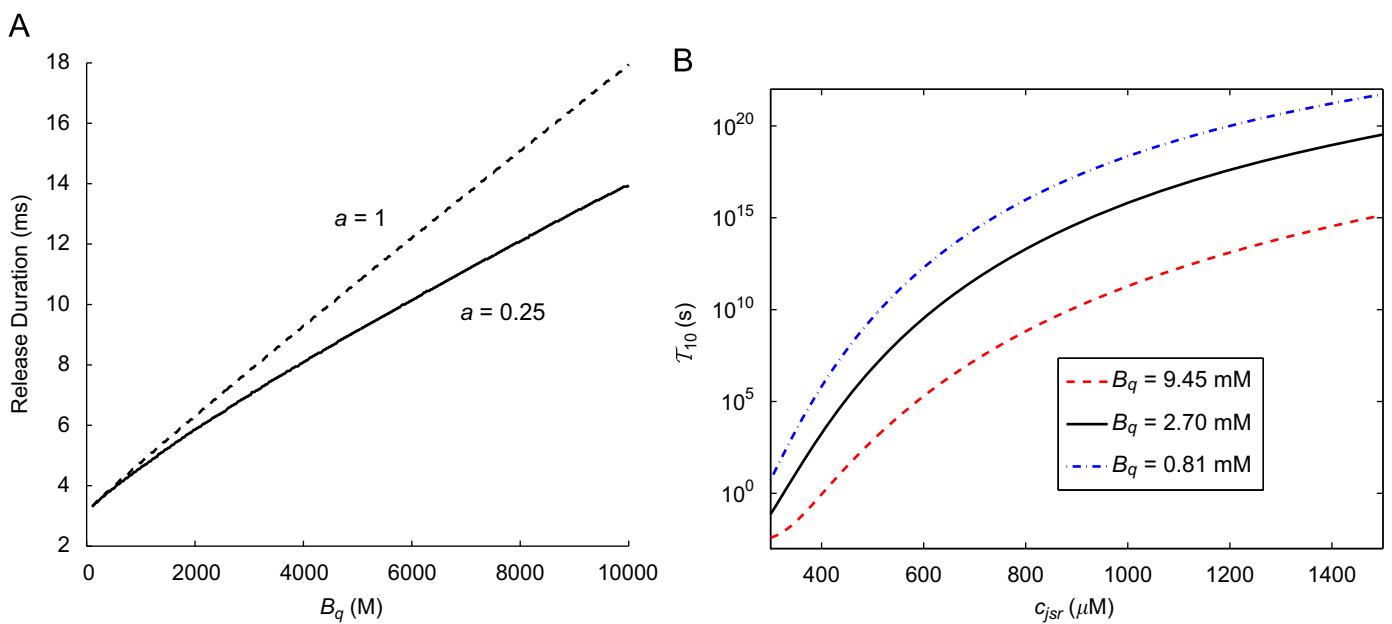


Fig. 10. Spark dynamics for different levels of CSQ expression when  $a < 1$ . Time course of different variables during a simulated deterministic calcium spark for three different values of  $B_q$  are shown: (A) fraction of open channels, (B) JSR calcium concentration, and (C) diadic calcium concentration.



**Fig. 11.** Deterministic calcium spark profiles with no luminal sensing ( $a=1$ ) where CSQ simply acts as a buffer alone. Time course of different variables during a simulated deterministic calcium spark for three values of  $B_q$  are shown: (A) fraction of open channels, (B) JSR calcium concentration, and (C) diadic calcium concentration.



**Fig. 12.** Dependence of spark termination on  $B_q$ : (A) release duration as a function of  $B_q$  for two different values of  $a$ . The release duration is computed by simulating the ODE system and finding the time when  $c_{jsr}$  reaches its minimum value and (B) the mean transition time  $\mathcal{T}_{10}$  as a function of  $c_{jsr}$  for three different  $B_q$  values.

shown in Fig. 12B, the mean waiting time for termination  $\mathcal{T}_{10}$  at each  $c_{jsr}$  value is shorter when  $B_q$  is higher.

#### 4.3. Effects of calsequestrin amount on spontaneous release

The effect of changing  $B_q$  on spontaneous spark generation can be studied by computing  $\mathcal{T}_{01}$ . When luminal sensing is not taken into consideration ( $a=1$ ), the spark switching time  $\mathcal{T}_{01}$  remains constant as plotted in Fig. 8 for any value of  $B_q$ . The results when  $a < 1$  are shown in Fig. 13. As the RyR open rate  $A(c, q)$  decreases when free CSQ level is increased, the occurrence of spontaneous sparks becomes less likely when the total CSQ amount is higher. This is specifically shown in Fig. 13A where the expected time to a spontaneous spark generation,  $\mathcal{T}_{01}$ , is plotted as a function of  $c_{jsr}$ . At high JSR calcium concentration, the changes in  $\mathcal{T}_{01}$  values for different  $B_q$  levels are not as prominent as for lower  $c_{jsr}$ . When JSR calcium is high, most of the CSQ molecules are bound to  $Ca^{2+}$  and do not interact with the RyR channels.

Our analysis thus indicates that increasing  $B_q$  has two effects. First, increasing the amount of luminal buffer prolongs the spark

duration, thus increasing the total amount of calcium released. The second effect is due to luminal sensing: with a higher amount of  $B_q$ , the level of free CSQ that interacts with RyR also increases, hence the spontaneous spark rate decreases (longer waiting time  $\mathcal{T}_{01}$ ). These results can be used to explain an experimental observation from Kubalova et al. (2004) which indicates that calcium wave velocity is constant regardless of the level of CSQ expression. When only the buffering effect is taken into consideration, the calcium wave velocity should grow as CSQ level is increased. When CSQ is higher, more  $Ca^{2+}$  is stored inside the JSR thus the amplitude of calcium spark increases hence calcium wave should propagate faster. However, when luminal sensing is taken into account, it is possible for the wave velocity to remain relatively constant regardless of the total CSQ amount. Once a release site has fired, the problem of finding the time of firing for the neighboring release site can be reduced to finding the spontaneous release time  $\mathcal{T}_{01}$  depending on the level of  $c_{jsr}$  at that particular release site. In Fig. 13B, we plot  $\mathcal{T}_{01}$  as a function of  $B_q$  for different  $c_{jsr}$  levels. When  $B_q$  is increased, the waiting time is also increased. This effect becomes more prominent when  $c_{jsr}$  is lowered, e.g. due to partial depletion of the NSR as the wave

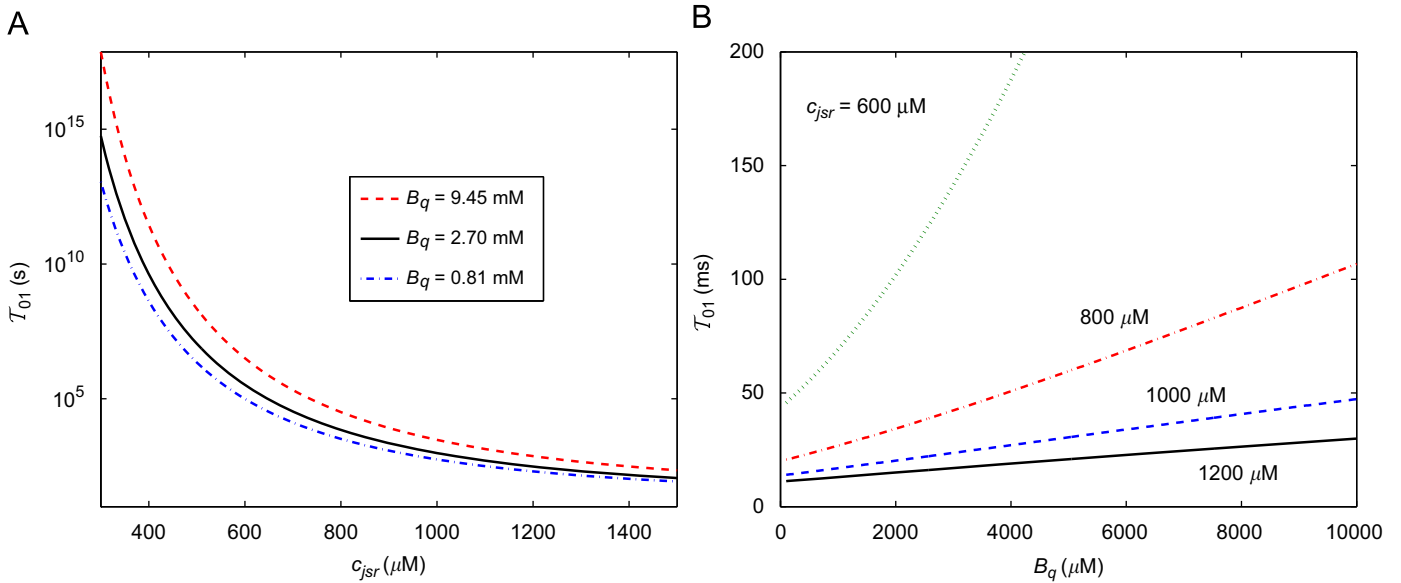


**Fig. 13.** Mean transition time for spark generation under varying  $B_q$  values.  $\mathcal{T}_{01}$  has dependence on  $B_q$  only when luminal sensing is taken into account,  $a < 1$ : (A)  $\mathcal{T}_{01}$  as a function of  $c_{jsr}$  for three different  $B_q$  values. A basal low value of myoplasmic calcium,  $c_{myo} = 0.1 \mu\text{M}$ , is used and (B)  $\mathcal{T}_{01}$  as a function of  $B_q$  for different  $c_{jsr}$  values. To reflect the condition under wave propagation, a higher value of  $c_{myo} = 0.8 \mu\text{M}$  is used.

propagates. Thus, as the basal spark rate is lower for large  $B_q$ , it is still possible for calcium wave to propagate more slowly even though each site releases a larger bolus of calcium.

#### 4.4. Effects of calsequestrin amount on spark regeneration

We now consider the effect of CSQ expression on the interspark interval. As before, our goal is to distinguish between the two effects of increasing  $B_q$ . First, when CSQ is higher, we find that the basal spark rate decreases thus the interspark interval is higher. Secondly, with increasing  $B_q$  value, more buffer is present thus a longer refilling period is needed to reach the same level of free JSR calcium. To study the contributions from each of these factors, we consider two different values of the bulk myoplasmic concentration,  $c_{myo}$ . We show that in low  $c_{myo}$  regime, the interspark interval is primarily determined by the basal spark rate at rest. Meanwhile, in the high  $c_{myo}$  regime, JSR refilling dynamics plays a more important role in determining the next spark time.

To determine the interspark interval at a particular CRU, we use a similar approach as the one used to find the stochastic spark duration in the previous section. Let  $t_{rel}$  be a random variable describing the time at which another spark is generated. The cumulative distribution function,  $P(t)$ , for  $t_{rel}$  follows the equation:

$$\frac{dP}{dt} = \frac{1}{\mathcal{T}_{01}(c_{jsr}(t))} (1 - P(t)). \quad (19)$$

The spark rate  $1/\mathcal{T}_{01}(c_{jsr}(t))$  evolves with time following the recovery dynamics of  $c_{jsr}$ . Solving this equation,

$$P(t) = 1 - \exp\left(-\int_0^t \frac{1}{\mathcal{T}_{01}(c_{jsr}(s))} ds\right), \quad (20)$$

and the probability density function is obtained by differentiating  $P(t)$  with respect to  $t$ ,

$$p(t) = \frac{1}{\tau_0(c_{jsr}(t))} \exp\left(-\int_0^t \frac{1}{\mathcal{T}_{01}(c_{jsr}(s))} ds\right). \quad (21)$$

The time course for  $c_{jsr}$  is then found by solving Eq. (13) using the quasi-equilibrium value of  $x_0(c_{jsr})$ . We wait for the next spark to

occur immediately after the first release event terminates. That is, we assume that initially JSR  $\text{Ca}^{2+}$  is at the critical termination  $c_{jsr}$  value from which it increases as refilling occurs. As the JSR load increases, the likelihood for another spark to occur also grows.

When  $c_{myo}$  is low, the recovery/refilling dynamics of  $c_{jsr}$  plays very little role in determining the next spark time. While  $c_{jsr}$  refilling occurs on the time-scale of 10s–100s of ms (e.g. see Figs. 10B and 11B), the mean waiting time for spark generation,  $\mathcal{T}_{01}$  is of the order of 1–10s of seconds. Thus in this case, the CSQ buffering effect does not affect the interspark interval. Rather, the dependence of the interspark interval on  $B_q$  can simply be accounted for by luminal sensing. Within the low  $c_{myo}$  regime, the next spark time  $t_{rel}$  closely follows an exponential distribution with rate  $1/\mathcal{T}_{01}(c_{jsr}^*)$  where  $c_{jsr}^*$  is the steady-state rest level of the JSR calcium. Indeed, the difference between the actual probability distribution for  $t_{rel}$ , as given in (20) and (21), is almost indistinguishable from the exponential distribution as shown in Fig. 14A. The mean interspark interval as a function of  $B_q$  for two different but low values of  $c_{myo}$  are shown in Fig. 14B. Results for  $a=1$  and  $a < 1$  are compared. Here, the mean interspark interval is defined as the sum of the spark duration (see Fig. 12) and the expected value of  $t_{rel}$  following the distribution given in (21). Although the spark duration and the JSR refilling time are both increasing functions of  $B_q$ , their values are small compared to the waiting time for the next spark  $t_{rel}$ . As a result without luminal sensing ( $a=1$ ), the interspark interval is approximately constant as  $B_q$  is varied. On the other hand, with  $a < 1$ , the interspark interval is an increasing function of  $B_q$  solely due to luminal sensing effect.

The JSR refilling process affects the interspark interval only when it is of the same time scale as the spark waiting time  $\mathcal{T}_{01}$ . This occurs when  $c_{myo}$  is high; then,  $\mathcal{T}_{01}$  drops to the order of 10s–100s of ms comparable to that of JSR refilling. The dynamics of  $c_{jsr}$  recovery as well as the distributions for the next spark time,  $t_{rel}$ , are shown in Fig. 15A. Three different  $B_q$  values are considered. In all cases, the peak of the PDF,  $p(t)$ , occurs before  $c_{jsr}$  is fully recovered. The mean interspark interval is an increasing function of  $B_q$  as shown in Fig. 15B. However, note that when  $a < 1$ ,  $\mathcal{T}_{01}$  at each  $c_{jsr}$  value also grows larger as  $B_q$  is increased. As a result, the CDF,  $P(t)$ , changes even more slowly for the high  $B_q$  case and

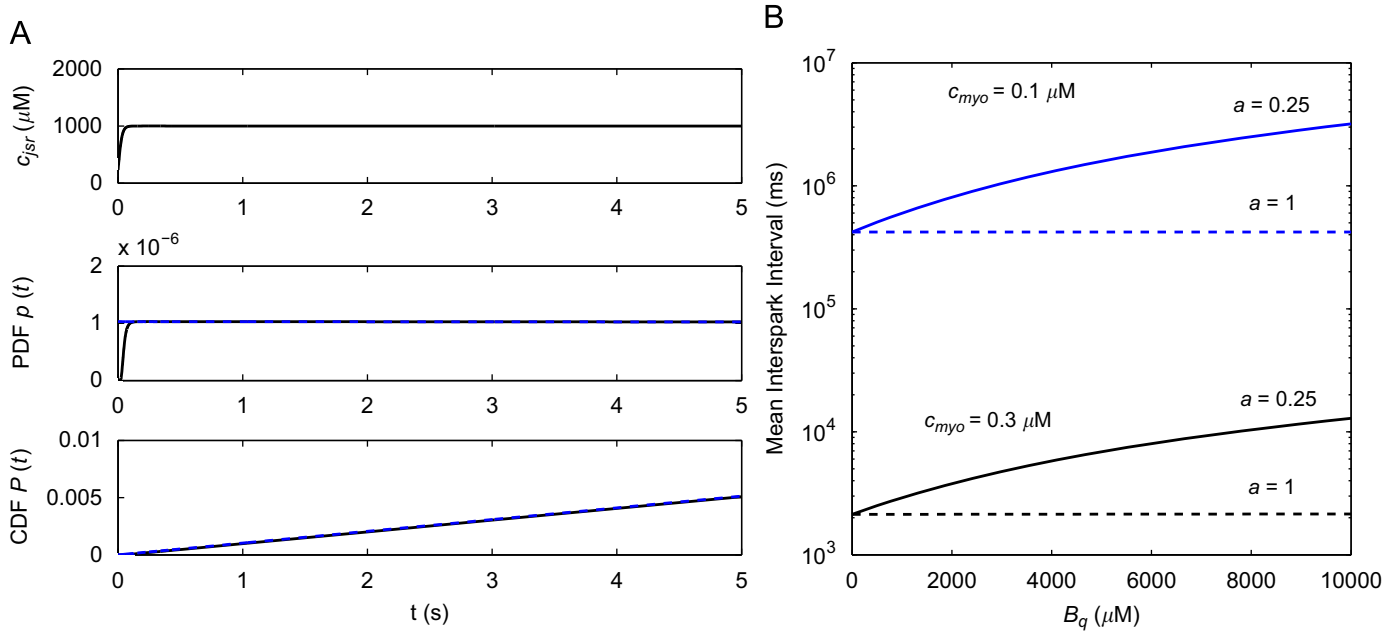


**Fig. 14.** Interspark interval at low  $c_{myo}$  is primarily determined by the mean spark time  $\mathcal{T}_{01}$  at steady-state  $c_{jsr}$ : (A) time course for the  $c_{jsr}$  and the probability functions  $p(t)$  and  $P(t)$  for the next spark time  $t_{rel}$  ( $B_q=2.7$  mM,  $c_{myo} = 0.1 \mu\text{M}$ ,  $a=0.25$ ). The approximations of the PDF and CDF using the exponential distribution with rate  $1/\mathcal{T}_{01}$  at  $c_{jsr} = 1000 \mu\text{M}$  are shown as a dashed line. Except for the early dynamics when  $c_{jsr}$  is refilling, the two curves are indistinguishable and (B) mean interspark interval as a function of  $B_q$ .

the corresponding PDF,  $p(t)$ , is broader as shown in Fig. 15A. Moreover, in Fig. 15B, the standard deviation for the next spark time  $t_{rel}$  is plotted as a function of  $B_q$ . When  $a < 1$ , the standard deviation grows larger as  $B_q$  is increased. Based on this, we predict that the interspark interval grows longer and becomes more irregular as  $B_q$  is increased. Note that this effect is not seen when luminal sensing is not taken into consideration. When  $a=1$ , the standard deviation remains relatively constant as  $B_q$  is varied as shown in Fig. 15B. Additionally, in Fig. 15C, we plotted the value of JSR calcium evaluated at the mean  $t_{rel}$  value. With luminal sensing ( $a < 1$ ), spark regeneration occurs, on average, at a relatively constant JSR calcium level regardless of the amount of  $B_q$ . Meanwhile when  $a=1$ , the average  $c_{jsr}$  value for spark regeneration decreases as  $B_q$  is increased. This is in agreement with the experimental observation of Kubalova et al. (2004) where JSR level is tracked by measuring fluorescent signal of Fluo-5 entrapped within the SR. Due to luminal sensing, the initiation of spontaneous calcium release occurs at a constant JSR calcium concentration regardless of the value of  $B_q$ , hence the total JSR calcium load.

#### 4.5. Deterministic oscillations under high cytoplasmic calcium

Recently, Stevens et al. (2009) showed that when permeabilized myocytes were exposed to high cytosolic calcium level, regular and periodic whole-cell calcium release occurred. Motivated by these findings, we investigate the behavior of the system under high cytoplasmic calcium level. Consistent with their findings, our CRU model also exhibits oscillations. Increasing  $c_{myo}$  results in a transition from an excitable CRU to an oscillatory unit. Results from simulations of the deterministic ODE system for three different values of  $c_{myo}$  are shown in Fig. 16. Within the oscillatory regime, increasing  $c_{myo}$  causes an increase in the oscillation frequency accompanied by a decrease in the amplitude of the oscillation, measured by changes in the JSR calcium level.

A full bifurcation diagram for the system is shown in Fig. 17A. When  $c_{myo}$  is low, the system forms an excitable system as discussed above. Within this regime, if  $c_{myo}$  lies below the saddle-node bifurcation point, labeled  $LP_U$  in Fig. 17A, there is only one equilibrium solution. For  $c_{myo}$  values between the two limit-point bifurcations, ( $LP_U, LP_L$ ), three equilibrium solutions exist but only the rest-level state, with the lowest steady state  $x$ -value, is stable. The rest equilibrium point loses stability through a subcritical Hopf bifurcation,  $HB_L$ , as  $c_{myo}$  is increased further. The subcritical Hopf bifurcation gives rise to a branch of periodic orbits which rises nearly vertically and is initially unstable but becomes stable at a saddle-node-of-periodics turning point. As the value of  $c_{myo}$  is increased further, a supercritical Hopf bifurcation  $HB_U$  is observed. The stability of the equilibrium point is regained, but the system is no longer excitable having high  $x$  and low  $c_{jsr}$  values. This corresponds to the state where the RyRs remain open and the JSR calcium level is at a constant low depleted level.

In Fig. 17B, we give a two-parameter bifurcation diagram which shows the range of  $c_{myo}$  for stable oscillation at different values of the total CSQ level,  $B_q$ . Specifically, the bifurcation points,  $HB_L$ ,  $LP_L$  and  $HB_U$ , are plotted as  $B_q$  is varied. For low  $B_q$ , oscillation onset occurs at a lower  $c_{myo}$  value and the oscillatory regime is narrow. As  $B_q$  is increased, both Hopf bifurcation points shift to higher  $c_{myo}$  values and the region of oscillation widened. This effect is consistent with the experimental findings (Stevens et al., 2009).

In comparison, however, we find that the region of oscillation in our CRU model is much narrower ( $c_{myo} = 1-2 \mu\text{M}$ ) compared to that in the experiments ( $1-50 \mu\text{M}$ ). Moreover, we find that increasing  $c_{myo}$  only increases the frequency of oscillation. Meanwhile, Stevens et al. (2009) observed that at high cytoplasmic  $\text{Ca}^{2+}$  concentration, the oscillation frequency drops lower with the JSR content remaining at a low level for an extended period of time. In general, the whole-cell oscillation also occurs at a much slower time scale (period of 1–10 s). The result obtained from our CRU model has several limitations. One important one is that it only reflects  $\text{Ca}^{2+}$  release within a single unit. All the

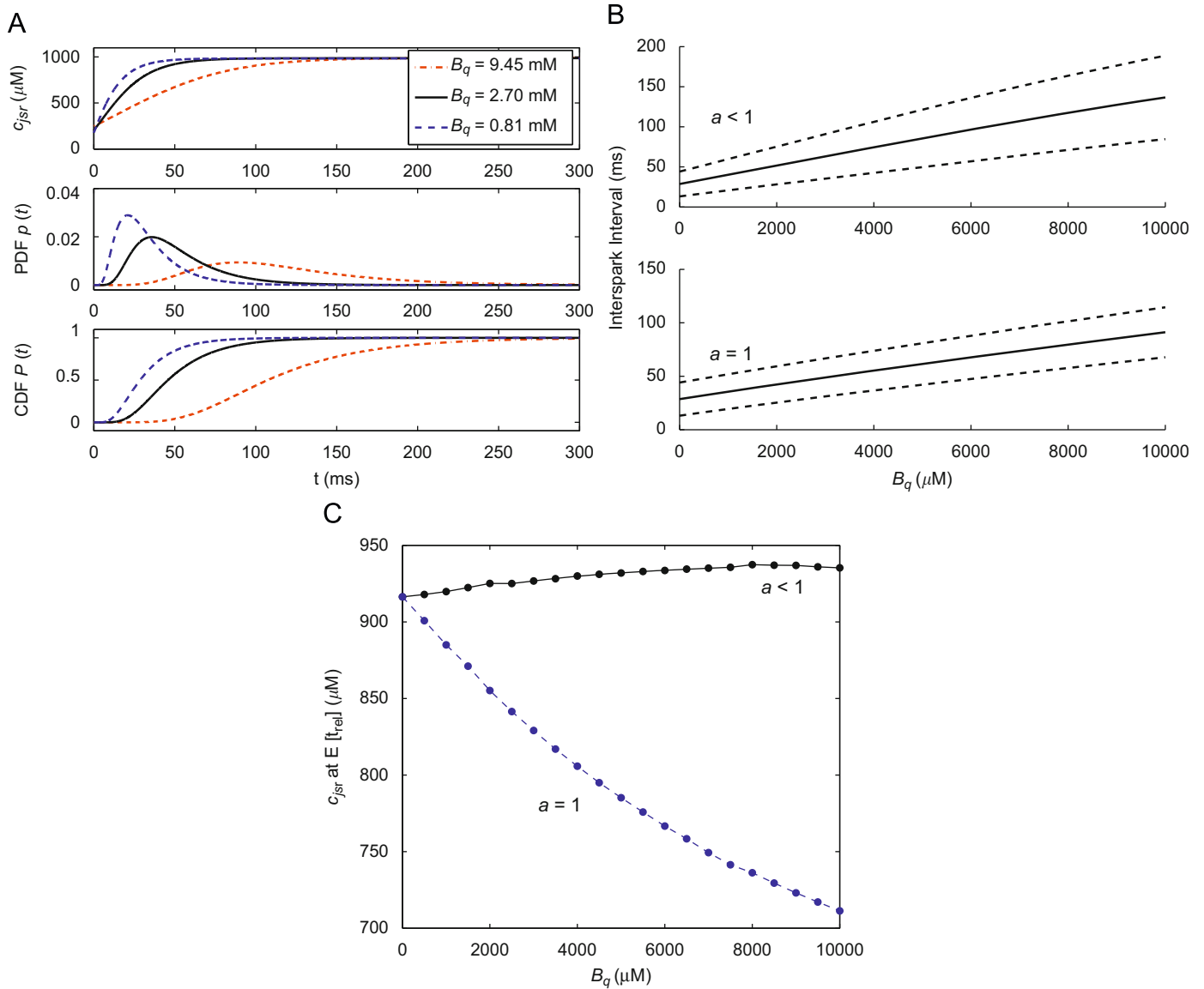


**Fig. 15.** Spark regeneration at high  $c_{myo}$  occurs at the same timescale as the JSR refilling process: (A) time course for the  $c_{jsr}$  and the probability functions  $p(t)$  and  $P(t)$  for the next spark time  $t_{rel}$  for three different values of  $B_q$  ( $c_{myo} = 0.8 \mu\text{M}$ ,  $a = 0.25$ ); (B) mean interspark interval as a function of  $B_q$  for  $a < 1$  and  $a = 1$ . The solid line indicates the mean while the dashed lines correspond to the mean  $\pm$  the standard deviation, both of which are computed using the probability distribution (21) and (C) JSR calcium level at mean spark regeneration time  $t_{rel}$ .

calculations presented here are obtained under fixed network SR concentration,  $c_{nsr}$ . The role of network SR depletion is important in the study of whole-cell events as shown in the global SR measurement shown by Stevens et al. (2009).

The limitation of our result when compared to experimental measurement may also shed light on the nature of the oscillations. Note that in our deterministic CRU system,  $c_{myo}$  affects only the  $x$ -nullcline while the value of  $c_{nsr}$  controls the  $c_{jsr}$ -nullcline only. At high  $c_{myo}$  value ( $> 3 \mu\text{M}$ ), the  $x$ -nullcline no longer has a cubic-like shape. If a whole-cell model were to be built by combining a number of CRU subsystems (see Hinch et al., 2004; Williams et al., 2007 for possible methods), then each individual unit would no longer act as an excitable system under high fixed cytoplasmic calcium concentration. Thus, any oscillation obtained is controlled by SR refilling dynamics rather than by the closing and openings of RyRs. Indeed, this also explains the nature of the slow oscillations observed experimentally. At a high level of  $c_{myo}$ , the RyR population remains open and the flux of calcium through the channel is dependent solely on SR calcium content.

## 5. Discussion

To study the elementary calcium release, or spark, we build a model of a calcium release unit where individual RyR activities are incorporated. A whole-cell model built by aggregating thousands of such release units would be expensive to simulate. We show that a full CRU model can be reduced to a two-state stochastic process. By using various asymptotic approximations, we are able to reduce the CRU model to a two-variable ODE system which displays excitability. This reflects the all-or-none nature of calcium release within each release unit. To consider the stochastic individual RyR activity, a birth–death process reflecting the number of open RyRs is considered. After solving the mean first passage time problem for the birth–death process, we compute the rate of stochastic spark generation and termination. The CRU can thereafter be written as a two-state stochastic process with transition rates obtained from solving the mean first passage time problems. One feature of our reduced CRU model is that the number of open RyRs can vary within each CRU state and

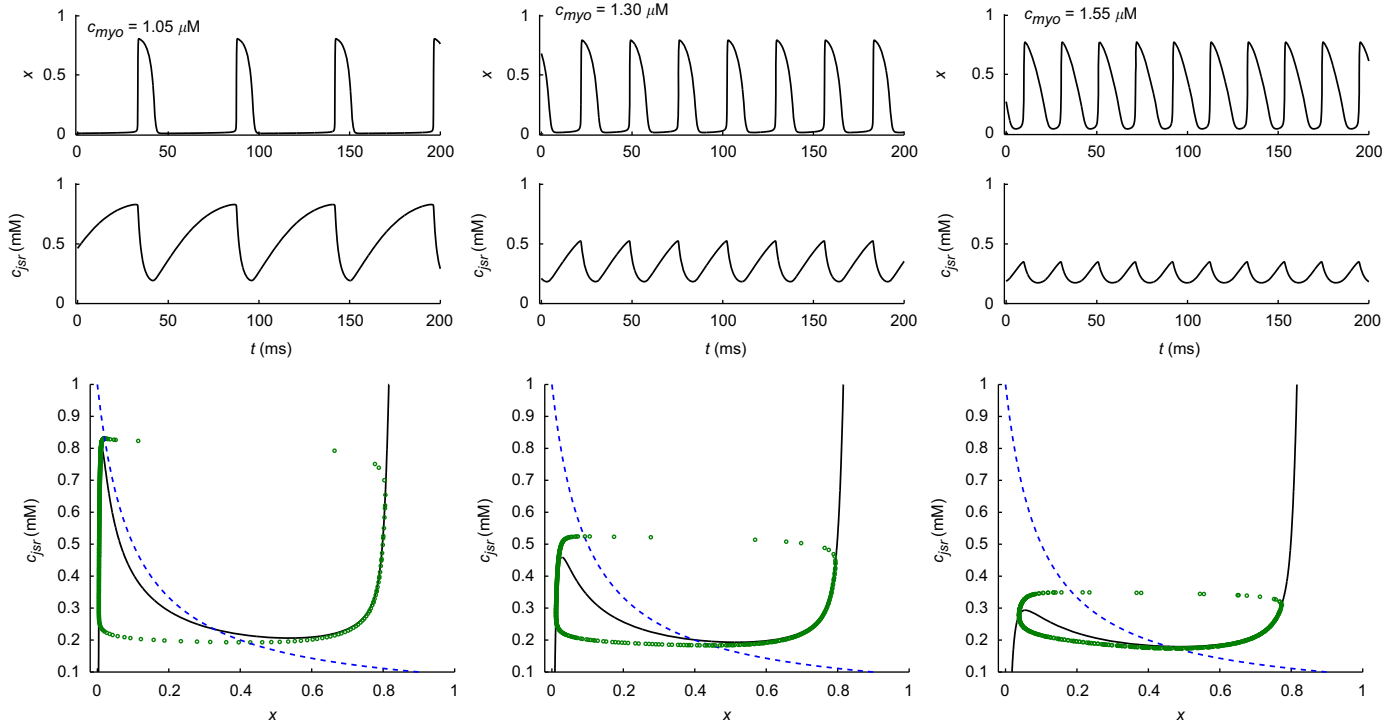


**Fig. 16.** Deterministic oscillations for high values of  $c_{myo}$ . Time trajectories are shown in the top and the corresponding phase planes with the nullclines drawn, are shown on the top.

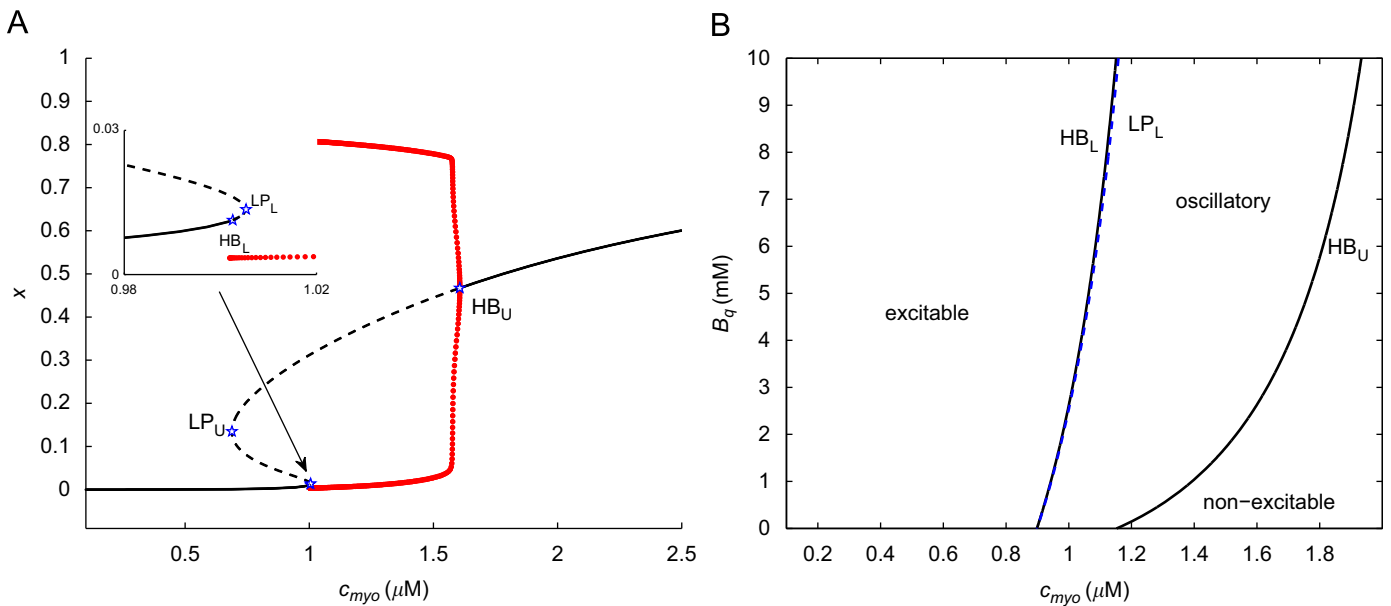


**Fig. 17.** Bifurcation diagrams for the deterministic CRU which show oscillatory regime of the system (A) bifurcation diagram for the standard model ( $\alpha=0.25$  and  $B_q = 2700 \mu\text{M}$ ) showing the equilibrium value of  $x$  as a function of  $c_{myo}$ . The stable branch of periodic solutions is shown in  $\bullet$  and the bifurcation points are indicated in  $\ast$ . As  $c_{myo}$  is increased, an oscillatory solution emerges at a subcritical Hopf bifurcation point ( $HB_L$ ). A limit point bifurcation ( $LP_L$ ) of the equilibrium solution can be found near the  $HB_L$  point. The periodic solution terminates at a supercritical Hopf point indicated as  $HB_U$ . (B) Two-parameter bifurcation diagram showing how the three bifurcation points,  $HB_L$ ,  $LP$  and  $HB_U$ , change as  $B_q$  is varied. Note that the pairs of limit-points and Hopf bifurcation points ( $HB_L$  and  $LP_L$ ,  $HB_U$  and  $LP_U$ ) each coalesce at a homoclinic bifurcation occurring at negative  $B_q$  values.

it is dependent upon the junctional SR and diadic space calcium concentration. This is in contrast to other models, such as in Williams et al. (2007), where a CRU is assumed to be a single two-state mega-channel.

The CRU reduction presented here is similar to that derived by Hinch (2004) and Hinch and Chapman (2005). However, rather than using asymptotic expansions, we used the full analytic solution of

the mean first passage time problem for a birth–death process describing the RyR openings. In either case, formulating a CRU as a two-state process is useful as it allows an extension for building a whole-cell model that can be formulated in terms of probability distribution functions for calcium release so that the likelihood of rare spontaneous events can be determined easily without having to generate a large sample of stochastic simulations.

Quasi-equilibrium approximations based on separations of time-scales are used in obtaining the two-state CRU reduction. Recently, Higgins et al. (2009) presented results which indicate that quasi-equilibrium assumptions introduces error into the statistics describing the activity of  $IP_3$  receptors. However, their results indicate that the largest error for the expected closing time is obtained when the approximations are taken in the model in which sequential binding of  $IP_3$  and  $Ca^{2+}$  is assumed. In that model, calcium-dependent inhibition only occurs when the channel is not bound to  $IP_3$ . In contrast, in the same version of the model in which sequential binding is not assumed, the error obtained is smaller. In our model, we assume very fast cooperative binding (four calcium to bind simultaneously). Moreover, there is no calcium dependent inactivation in our model thus we do not expect the quasi-equilibria approximations to affect the statistics of closing time as strongly. However, we have not explored the effect of sequential  $Ca^{2+}$  binding to RyR on the statistics of channel activity. To include sequential binding of calcium will introduce a large single channel model (a sixteen state model assuming four calcium binding sites). As a result, analytical and computational work on clusters with high number of channels will be intractable.

Parameter values in our CRU model are taken from existing models (Sobie et al., 2002; Hinch, 2004). One critical parameter which we fixed in our model is the maximum CRU  $Ca^{2+}$  conductance,  $g_{max}$ . This parameter is defined to be equal to the sum of all RyR conductance, i.e.  $g_{max} = N \cdot g_R$  where  $N$  is the total number of channels per CRU and  $g_R$  is the single channel conductance. Using the values listed in Table 1, we note that the single channel conductance is approximately one order of magnitude lower than the one that had been reported in an experimental studies of RyR (Mejía-Alvarez et al., 1999). However, this deduced value is also dependent on the number of channels within a CRU which has been reported to vary from 10 to 200 RyRs (Inoue and Bridge, 2005; Franzini-Armstrong et al., 1999). We have also checked our result under higher value of  $g_{max}$  (results not shown). Increasing  $g_{max}$  by 10 fold, we obtain similar result in that we still see excitability and oscillation and the system does not become unexcitable. The spark dynamics and statistics change and the region of oscillation is shifted towards higher cytoplasmic  $Ca^{2+}$  sensitivity, however, the qualitative behavior remains.

Having obtained a tractable and simplified CRU description, we then use it to study in details how calsequestrin mediates changes in calcium release within a CRU. We incorporate the luminal sensing effect into a mechanistic model of RyR–CSQ interaction by assuming that the open rate of a RyR decreases when the receptor is bound to CSQ. This reflects the fact that CSQ, through its interaction with Junctin and Triadin-1, desensitizes the RyR from cytosolic calcium dependent activation. A similar model of RyR–CSQ interaction which further includes the effect of CSQ polymerization under varying luminal calcium concentration, was recently presented by Restrepo et al. (2008). They used their model to study calcium alternans in a whole-cell system which consists of a large number of coupled CRUs. Meanwhile, the focus of our effort is to study in more detail the effect of changing CSQ expression on spark properties. In particular, in this study, we are able to distinguish between buffering and luminal sensing effects of CSQ. Moreover, using asymptotic reductions and mean first passage time calculations, we are able to obtain a CRU description that is computationally cheap to simulate and hence analyze. Our reduction can easily be incorporated to larger whole-cell models (Restrepo et al., 2008; Williams et al., 2007).

Consistent with experimental observations (Kubalova et al., 2004; Terentyev et al., 2003), we observe that the level of CSQ expression modulates basic calcium spark properties through

buffering effects. Increasing CSQ expression increases the spark duration, the amount of calcium released, and the JSR refilling period. Due to luminal sensing, we find that increasing the CSQ level depresses the basal spontaneous spark rate at rest condition. In addition, we show that under basal conditions (low bulk myoplasmic calcium), the dependence of the interspark interval on the amount of CSQ expression is simply determined by the luminal sensing effect. Within this regime, the mean spark generation time is much larger than the JSR refilling period so that the contribution of the buffering effect in determining the interspark interval is minimal. Next, we also find from our calculation that the critical JSR calcium concentration at which calcium release terminates, is dependent on the level of CSQ. Over-expression of CSQ causes release to terminate at a slightly higher JSR concentration.

In this paper, our aim is to quantify the effect of luminal sensing using the simplest mechanistic model of RyR–CSQ interaction. We thus do not include the effect of dynamics of CSQ binding/unbinding to RyR and instead use a quasi-equilibrium approximation to study how CSQ level desensitizes the RyR by changing the open rate instantaneously. Moreover, we do not take into consideration the effect of CSQ polymerization under varying JSR calcium concentration. Park et al. (2004) showed that under high JSR calcium, calsequestrin forms dimers and multimers. These polymer forms serve as a stronger calcium buffer as they are able to bind more calcium. Mutation that disrupts calsequestrin polymerization has also been associated with CPVT (Terentyev et al., 2008). These effects can be important and affect the calcium release process significantly. The model proposed by Restrepo et al. (2008) takes into consideration these different factors. However, a detail study on how each of these modulate calcium release and spark generation has not been performed.

We also use our calculations on spark rate and size to explain an experimental finding by Kubalova et al. (2004) which indicates that the velocity of propagation for calcium waves does not seem to be affected by CSQ expression. Although increasing CSQ expression increases the spark duration thus the amount of calcium released, the spark rate at each individual CRU decreases due to luminal sensing. We acknowledge the fact that this result is applicable for a single CRU. Translation to the whole-cell calcium wave may not be direct. A full calculation which tracks bulk cytoplasmic and NSR calcium levels and allows for the interactions and couplings between CRUs is necessary to study whole-cell events. A more careful study of whole-cell wave propagation can be accomplished by putting our stochastic CRU reduction into the stochastic fire-diffuse-fire model for  $Ca^{2+}$  waves described in Keener (2006) though additional dynamic variables for the SR concentration need to be included. Another possibility is to incorporate RyR luminal sensing, albeit phenomenologically, into a deterministic bidomain threshold model for wave propagation (Thul et al., 2008).

Finally, we show that by increasing the cytoplasmic calcium concentration, the CRU model exhibit deterministic oscillation. A transition from an excitable to an oscillatory system is observed. A form of coherence resonance in the stochastic CRU system was also observed: for cytoplasmic calcium concentration below the deterministic onset point (Hopf bifurcation), the interspark interval follows a bell-shaped like distribution (see Fig. 15A). In comparison to experimental findings by Stevens et al. (2009), however, the range of cytoplasmic calcium for oscillation in our mathematical model is very narrow. We again note that the result presented in this paper focuses on a single CRU. The role of network SR depletion has not been studied. We propose that the timescale of SR refilling controls the slow oscillation observed experimentally since oscillations caused by periodic opening and closing of RyRs occur at a much faster timescale as observed in our deterministic CRU system.

Our CRU model is based on the local control model which was initially proposed by Sobie et al. (2002) and further analyzed by Hinch (2004). Here, a CRU acts as an excitable system under basal condition. In a similar system of calcium regulation involving the IP<sub>3</sub> receptor (IPR), Thul and Falcke (2004, 2006) proposed that the cell is composed of local bistable units rather than excitable ones. They proposed that oscillations can be generated using deterministic models only if the IPRs are exposed to calcium concentration that are close to its calcium activation constant (0.1–10 μM) while in reality, local concentration near open IPRs reached values that are much higher (25–170 μM). Using known IPR kinetics parameter values, the deterministic system does not exhibit excitability or oscillation except for a very narrow range of IP<sub>3</sub> level. However, the underlying stationary distribution of the full stochastic system is bistable with one mode reflecting low calcium concentration with little release, and another with high calcium concentration with large release. They propose that whole-cell oscillation results due to stochastic transition, induced for example due to random single-channel activities, between these two potentials. It is possible that under high cytoplasmic calcium concentration, the CRU forms a stochastic bistable system and the oscillation observed by Stevens et al. (2009) follows the mechanism proposed by Thul and Falcke (2004, 2006). However, we do not observe this behavior using the parameter values used in the standard local control model. A thorough exploration of the parameter space will be needed to further study oscillations under high fixed cytoplasmic calcium concentration.

**Acknowledgment**

This research was supported in part by NSF Grant DMS-0718036.

**Appendix A. Birth death process for open RyRs**

The behavior of a cluster of  $N$  RyRs in the CRU can be described by the birth–death process (11) for  $S_n$ , a state of having  $n$  number of open channels. The corresponding master equations for  $p_n(t)$ , the probability of being in state  $S_n$  at time  $t$ , are

$$\frac{dp_n}{dt} = \alpha_{n-1}p_{n-1} - \beta_n p_n + \beta_{n+1}p_{n+1} - \alpha_n p_n, \tag{A.1}$$

where  $n=1, 2, \dots, N-1$  and

$$\frac{dp_0}{dt} = -\alpha_0 p_0 + \beta_1 p_1, \quad \frac{dp_N}{dt} = \alpha_{N-1}p_{N-1} - \beta_N p_N. \tag{A.2}$$

We first treat  $c_{jsr}$  as a parameter before considering its dynamics. In terms of steady-state solutions, excitability in the deterministic system corresponds to the fact that the stationary distribution  $p_n^*$  is bimodal. Following the calculation given for a general birth death process in Gardiner (2003), it can be shown that the stationary distribution satisfies

$$p_n^* = p_0^* \prod_{i=0}^{n-1} \frac{\alpha_i}{\beta_{i+1}} = p_0^* \binom{N}{n} \frac{1}{\beta^n} \prod_{i=0}^{n-1} \alpha(c_{ds}(i)) \tag{A.3}$$

for  $n=1,2,\dots,N$  and  $p_0^*$  is found by normalizing so that the distribution sums to one,

$$p_0^* = \left( 1 + \sum_{n=1}^N \binom{N}{n} \frac{1}{\beta^n} \prod_{i=0}^{n-1} \alpha(c_{ds}(i)) \right)^{-1}. \tag{A.4}$$

Plots of the steady-state distributions as  $c_{jsr}$  is varied are given in Fig. 18A. The steady-state distribution is bimodal as shown more clearly on a semilog axis in Fig. 18B. The first peak of  $p_n^*$  is at  $n=0$  and the second one is at a larger  $n$  which we refer to as  $n_1$ .

Changes in  $c_{jsr}$  affect the steady-state distribution by shifting its most likely position. When  $c_{jsr}$  is high, the maximum of  $p_n^*$  lies at  $n_1$  but as  $c_{jsr}$  decreases,  $p_0^*$  increases so the most likely position switches to 0. As the JSR content becomes partially depleted, termination of calcium release becomes more likely. Bimodality of  $p_n^*$  is gradually lost as  $c_{jsr}$  is decreased towards the critical  $c_{jsr}$  value so that the distribution only has one maximum at 0 as shown in Fig. 18B for  $c_{jsr} = 200 \mu\text{M}$ .

**Appendix B. Mean first passage time calculation**

Following the bimodality in the stationary distribution, we now reduce the Markov-chain description in Eq. (11) to a two-state stochastic process corresponding to the two local maxima of  $p_n$  or the lower and upper branches of the  $dx/dt$  nullclines in the context of the continuous model. The rates of transition between the two states are obtained from by solving the mean first passage time problem as detailed below.

At a particular  $c_{jsr}$  value, the expected waiting time for spark generation, or the 0 to  $n_1$  transition, can be computed by solving the mean first exit time problem for the birth–death process (11).

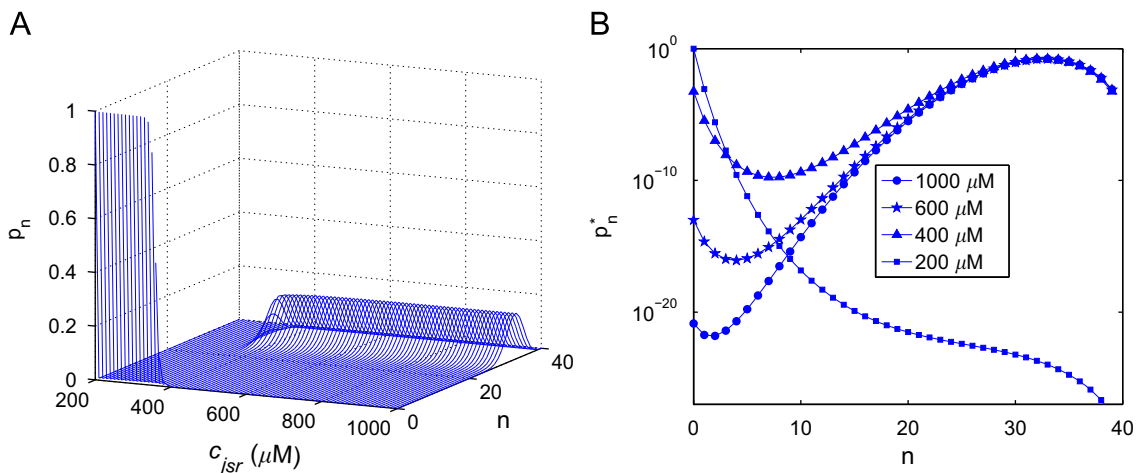


**Fig. 18.** Steady-state distributions and its dependence on  $c_{jsr}$ : (A) steady-state distributions of the master equations,  $p_n^*$  plotted as functions of  $c_{jsr}$  and (B)  $p_n^*$  for  $c_{jsr} = 200, 400, 600,$  and  $1000 \mu\text{M}$  plotted on a log scale to show that the distribution is bimodal but the peak at  $n_1$  is gradually lost as JSR  $\text{Ca}^{2+}$  decreases.

Suppose that the system starts at a particular state  $S_j$ . Assuming that  $n_L < j < n_R$ , the mean first exit time,  $\tau_j$ , from the interval  $[n_L, n_R]$  satisfies the difference equation,

$$\alpha_j(\tau_{j+1} - \tau_j) + \beta_j(\tau_{j-1} - \tau_j) = -1. \quad (B.1)$$

A derivation of this relationship involves the backward master equation and can be found in textbooks such as Gardiner (2003).  $\tau(j)$  can be found by solving the resulting system of algebraic equations with appropriate boundary conditions at  $n_L$  and  $n_R$ .

Applying this specifically to our problem, the expected time for spontaneous spark generation can be found by first solving the difference equations (B.1) above for  $0 < j < n_1$  with a reflecting boundary at 0 and an absorbing boundary at  $n_1$ ,

$$\tau_{-1} = \tau_0 \quad \text{and} \quad \tau_{n_1} = 0. \quad (B.2)$$

The solution to this system of equations can be obtained as follows. A similar derivation can also be found in Gardiner (2003). First, let  $u_j = \tau_{j+1} - \tau_j$ , so

$$\alpha_j u_j - \beta_j u_{j-1} = -1. \quad (B.3)$$

The reflecting boundary condition at  $S_0$  then gives  $u_{-1} = 0$  and  $u_0 = -1/\alpha_0$ . From this, the remaining  $u_j$  can be solved sequentially,

$$u_1 = -\frac{1}{\alpha_1} - \frac{1}{\alpha_0} \phi_1,$$

$$u_2 = -\frac{1}{\alpha_2} - \frac{1}{\alpha_1} \phi_2 - \frac{1}{\alpha_0} \phi_1 \phi_2,$$

⋮

$$u_j = -\frac{1}{\alpha_j} - \sum_{k=0}^{j-1} \frac{1}{\alpha_k} \prod_{i=k+1}^j \phi_i, \quad (B.4)$$

where  $\phi_i = \beta_i/\alpha_i$ . Having solved for  $u_j$ ,  $\tau_j$  can then be determined by first using the absorbing boundary condition at  $S_{n_1}$ . Since  $\tau_{n_1} = 0$ ,  $\tau_{n_1-1} = -u_{n_1-1}$ . Thus,  $\tau_{n_1-2} = \tau_{n_1-1} - u_{n_1-2} = u_{n_1-2} - u_{n_1-2}$ , and so on. This results finally in

$$\tau_j = -\sum_{n=j}^{n_1-1} u_n = \sum_{n=j}^{n_1-1} \left( \frac{1}{\alpha_n} + \sum_{k=0}^{n-1} \frac{1}{\alpha_k} \prod_{i=k+1}^n \phi_i \right). \quad (B.5)$$

We consider the mean spark generation time,  $\mathcal{T}_{01}$ , by applying the previous equation to  $j=0$ . That is, we assume that the initial state of the system is at  $S_0$  where no RyR channel is open. With this,

$$\mathcal{T}_{01} = \sum_{n=0}^{n_1-1} \left( \frac{1}{\alpha_n} + \sum_{k=0}^{n-1} \frac{1}{\alpha_k} \prod_{i=k+1}^n \phi_i \right). \quad (B.6)$$

The transition from  $S_{n_1}$  to  $S_0$  is related to spark termination. The mean first passage time itself does not reflect the spark termination time accurately as  $C_{jsr}$  dynamics need to be taken into consideration. However, the mean transition rate as a function of  $C_{jsr}$  has to be determined before the full system can be analyzed. The transition time can be computed using the same system of Eqs. (B.1) but with the boundary conditions,

$$\tau_0 = 0 \quad \text{and} \quad \tau_{N+1} = \tau_N, \quad (B.7)$$

so that now,  $S_0$  is an absorbing state and  $S_N$  is a reflecting state. Using similar steps as before and applying the initial condition to be at  $n_1$  yields  $\mathcal{T}_{10}$ ,

$$\mathcal{T}_{10} = \sum_{n=1}^{n_1} \left( \frac{1}{\beta_n} + \sum_{k=n+1}^N \frac{1}{\beta_k} \prod_{i=n}^{k-1} \alpha_i \right). \quad (B.8)$$

## References

- Beard, N.A., Casarotto, M.G., Wei, L., Varsanyi, M., Laver, D.R., Dulhunty, A.F., 2005. Regulation of ryanodine receptors by calsequestrin: effect of high luminal  $\text{Ca}^{2+}$  and phosphorylation. *Biophys. J.* 88, 3444–3454.
- Beltran, M., Barrientos, G., Hidalgo, C., 2006. Fast kinetics of calcium dissociation from calsequestrin. *Biol. Res.* 39, 493–503.
- Bers, D.M., 1991. Excitation–Contraction Coupling and Cardiac Contractile Force. Kluwer Academic Press, Dordrecht, Netherlands.
- Franzini-Armstrong, C., Protasi, F., Ramesh, V., 1999. Shape, size, and distribution of  $\text{Ca}^{2+}$  release units and couplons in skeletal and cardiac muscles. *Biophys. J.* 77, 1528–1539.
- Gardiner, C.W., 2003. Handbook of Stochastic Methods for Physics, Chemistry and the Natural Sciences, third ed Springer-Verlag, New York.
- Greenstein, J.L., Hinch, R., Winslow, R.L., 2006. Mechanisms of excitation–contraction coupling in an integrative model of the cardiac ventricular myocyte. *Biophys. J.* 90, 77–91.
- Greenstein, J.L., Winslow, R.L., 2002. An integrative model of the cardiac ventricular myocyte incorporating local control of  $\text{Ca}^{2+}$  release. *Biophys. J.* 83, 2918–2945.
- Gyorke, I., Gyorke, S., 1998. Regulation of the cardiac ryanodine receptor channel by luminal  $\text{Ca}^{2+}$  involves luminal  $\text{Ca}^{2+}$  sensing sites. *Biophys. J.* 75, 2801–2810.
- Gyorke, I., Hester, N., Jones, L., Gyorke, S., 2004. The role of calsequestrin, triadin, and junction in conferring cardiac ryanodine receptor responsiveness to luminal calcium. *Biophys. J.* 86, 2121–2128.
- Higgins, E.R., Schmidle, H., Falcke, M., 2009. Waiting time distributions for clusters of  $\text{IP}_3$  receptors. *J. Theor. Biol.* 259 (2), 338–349.
- Hinch, R., 2004. A mathematical analysis of the generation and termination of calcium sparks. *Biophys. J.* 86, 2121–2128.
- Hinch, R., Chapman, S., 2005. Exponentially slow transitions on a Markov chain: the frequency of calcium sparks. *Eur. J. Appl. Math.* 16, 1–20.
- Hinch, R., Greenstein, J.L., Tanskanen, A.J., Xu, L., Winslow, R.L., 2004. A simplified local control model of calcium-induced calcium release in cardiac ventricular myocyte. *Biophys. J.* 87, 3723–3736.
- Inoue, M., Bridge, J., 2005. Variability in couplon size in rabbit ventricular myocytes. *Biophys. J.* 89, 3102–3110.
- Keener, J.P., 2006. Stochastic calcium oscillations. *Math. Med. Biol.* 23, 1–25.
- Keener, J.P., Sneyd, J., 1998. Mathematical Physiology. Springer-Verlag, New York.
- Kubalova, Z., Gyorke, I., Terentyeva, R., Viatchenko-Karpinski, S., Terentyev, D., Williams, S.C., Gyorke, S., 2004. Modulation of cytosolic and intra-sarcoplasmic reticulum calcium waves by calsequestrin in rat cardiac myocytes. *J. Physiol.* 561, 515–524.
- Lahat, H., Pras, E., Olender, T., Avidan, N., Ben-Asher, E., Man, O., Levy-Nissenbaum, E., Khoury, A., Lorber, A., Goldman, B., Lancet, D., Eldar, M., 2001. A missense mutation in a highly conserved region of CASQ2 is associated with autosomal recessive catecholamine-induced polymorphic ventricular tachycardia in Bedouin families from Israel. *Am. J. Hum. Genet.* 69, 1378–1384.
- Mejía-Alvarez, R., Kettlun, C., Ríos, E., Stern, M., Fill, M., 1999. Unitary  $\text{Ca}^{2+}$  current through cardiac ryanodine receptor channels under quasi-physiological ionic conditions. *J. Gen. Physiol.* 113 (2), 177–186.
- Park, H., Park, I.Y., Kim, E., Youn, B., Fields, K., Dunker, A.K., Kang, C., 2004. Comparing skeletal and cardiac calsequestrin structures and their calcium binding. *J. Biol. Chem.* 279, 18026–18033.
- Restrepo, J.G., Weiss, J.N., Karma, A., 2008. Calsequestrin-mediated mechanism for cellular calcium transient alternans. *Biophys. J.* 95, 3767–3789.
- Rice, J.J., Jafri, M.S., Winslow, R.L., 2002. Modeling gain and gradedness of  $\text{Ca}^{2+}$  release in the functional unit of the cardiac diadic space. *Biophys. J.* 77, 1871–1884.
- Shannon, T.R., Ginsburg, K.S., Bers, D.M., 2000. Potentiation of fractional sarcoplasmic reticulum calcium release by total and free intracellular sarcoplasmic reticulum calcium concentration. *Biophys. J.* 78, 334–343.
- Shannon, T.R., Wang, F., Puglisi, J., Weber, C., Bers, D.M., 2004. A mathematical treatment of integrated  $\text{Ca}^{2+}$  dynamics within the ventricular myocyte. *Biophys. J.* 87, 3351–3371.
- Sobie, E., Dilly, K., dos Santos Cruz, J., Lederer, W., Jafri, M., 2002. Termination of cardiac  $\text{Ca}^{2+}$  sparks: an investigative mathematical model of calcium-induced calcium release. *Biophys. J.* 83, 59–78.
- Stern, M.D., 1992. Theory of excitation-coupling in cardiac muscle. *Biophys. J.* 63, 497–517.
- Stevens, S.C., Terentyev, D., Kalyanasundaram, A., Periasamy, M., Gyorke, S., 2009. Intra-sarcoplasmic reticulum  $\text{Ca}^{2+}$  oscillations are driven by dynamic regulation of ryanodine receptor function by luminal  $\text{Ca}^{2+}$  in cardiomyocytes. *J. Physiol.* 587, 4863–4872.
- Swietach, P., Spitzer, K.W., Vaughan-Jones, R.D., 2008.  $\text{Ca}^{2+}$ -mobility in the sarcoplasmic reticulum of ventricular myocytes is low. *Biophys. J.* 95, 1412–1427.
- Tanskanen, A.J., Greenstein, J.L., Chen, A., Sun, S.X., Winslow, R.L., 2007. Protein geometry and placement in the cardiac dyad influence macroscopic properties of calcium-induced calcium release. *Biophys. J.* 92, 3379–3396.
- Terentyev, D., Kubalova, Z., Valle, G., Nori, A., Vedamoorthy, S., Terentyeva, R., Viatchenko-Karpinski, S., Bers, D.M., Williams, S.C., Volpe, P., Gyorke, S., 2008. Modulation of sr ca release by luminal ca and calsequestrin in cardiac myocytes: effects of casq2 mutations linked to sudden cardiac death. *Biophys. J.* 95, 2037–2048.

- Terentyev, D., Nori, A., Santoro, M., Viatchenko-Karpinski, S., Kubalova, Z., Gyorke, I., Terentyeva, R., Vedamoorthyrao, S., Blom, N., Valle, G., Napolitano, C., Williams, S., Volpe, P., Priori, S., Gyorke, S., 2006. Abnormal interactions of calsequestrin with the ryanodine receptor calcium release channel complex linked to exercise-induced sudden cardiac death. *Circ. Res.* 98, 1151–1158.
- Terentyev, D., Viatchenko-Karpinski, S., Gyorke, I., Volpe, P., Williams, S., Gyorke, S., 2003. Calsequestrin determines the functional size and stability of cardiac intracellular calcium stores: mechanism for hereditary arrhythmia. *Proc. Natl. Acad. Sci. USA* 100, 11759–11764.
- Terentyev, D., Viatchenko-Karpinski, S., Valdivia, H., Escobar, A., Gyorke, S., 2002. Luminal  $Ca^{2+}$  controls termination and refractory behavior of  $Ca^{2+}$ -induced  $Ca^{2+}$  release in cardiac myocytes. *Circ. Res.* 91, 414–420.
- Thul, R., Falcke, M., 2004. Stability of membrane bound reactions. *Phys. Rev. Lett.* 93, 188103.
- Thul, R., Falcke, M., 2006. Frequency of elemental events of intracellular  $Ca^{2+}$  dynamics. *Phys. Rev. E* 73, 061923.
- Thul, R., Smith, G.D., Coombes, S., 2008. A bidomain threshold model of propagating calcium waves. *J. Math. Biol.* 56, 435–463.
- Viatchenko-Karpinski, S., Terentyev, D., Gyorke, I., Terentyeva, R., Volpe, P., Priori, S.G., Napolitano, C., Nori, A., Williams, S.C., Gyorke, S., 2004. Abnormal calcium signaling and sudden cardiac death associated with mutation of calsequestrin. *Circ. Res.* 94, 471–477.
- Williams, G.S.B., Huertas, M.A., Sobie, E.A., Jafri, M.S., Smith, G.D., 2007. A probability density approach to modeling local control of calcium-induced calcium release in cardiac myocytes. *Biophys. J.* 92, 2311–2328.